ORIGINAL PAPER

Internal resonance and energy transfer of a cable-stayed beam with a tuned mass damper

Xiaoyang Su · Houjun Kang 🅓 **· Tieding Guo · Yunyue Cong**

Abstract This study considers a novel nonlinear system, namely a cable-stayed beam with a tuned mass damper (cable-beam-TMD model), allowing the description of energy transfer among the beam, cable and TMD. In this system, the vibration of the TMD is involved and one-to-one-to-one internal resonance among the modes of the beam, cable and TMD is investigated when external primary resonance of the beam occurs. Galerkin's method is utilized to discretize the equations of motion of the beam and cable. In this way, a set of ordinary differential equations are derived, which are solved by the method of multiple time scales. Then the steady-state solutions of the system are obtained by using Newton–Raphson method and continued by pseudo-arclength algorithm. The response curves, time histories and phase portraits are provided to explore the effect of the TMD on the nonlinear behaviors of the model. Meanwhile, a partially coupled system, namely a cable-beam-TMD model ignoring the vibration of the TMD, is also studied. The nonlinear characteristics of the two cases are compared with each other. The results reveal the occurrence of energy transfer among the beam, cable and TMD.

X. Su · H. Kang (✉)
Key Laboratory of Disaster Prevention and Structural Safety of Ministry of Education, Guangxi University, Nanning 530004, Guangxi, China
e-mail: houjun_kang@163.com

X. Su
e-mail: su_xiaoyang@hnu.edu.cn

X. Su · H. Kang
College of Civil Engineering, Hunan University, Changsha 410082, Hunan, China

X. Su · H. Kang · T. Guo · Y. Cong
School of Civil Engineering and Architecture, Guangxi University, Nanning 530004, Guangxi, China

X. Su · H. Kang · T. Guo · Y. Cong
Scientific Research Center of Engineering Mechanics, Guangxi University, Nanning 530004, Guangxi, China

X. Su · H. Kang · T. Guo · Y. Cong
Guangxi Key Laboratory of Disaster Prevention and Engineering Safety, Guangxi University, Nanning 530004, Guangxi, China

1 Introduction

Cable-supported systems [1, 2], especially cable-stayed bridges, are extensively used in cross-sea or cross-valley projects throughout the world [3]. With the continuous progress and improvement of technology, the span of cable-stayed bridges has exceeded one

thousand meters. The ensuing problem is that the nonlinear dynamics of the cable-stayed bridge are more prominent, which has received a considerable number of attentions.

Due to the complexity of the dynamics of the cable-stayed bridge, the researches on nonlinear dynamics of the cable-stayed bridge are mainly devoted to substructures, such as the cable [4, 5] and cable-stayed beam [6]. Cable dynamics has a long and rich history and can be traced back to the classic monograph by Irvine [7]. Afterwards, cable's problems have been widely studied by many researchers in the last few decades [8–13]. Although a single-cable model can reveal some characteristics of the cable-stayed bridge, however, it cannot consider the coupling interaction between the cable and bridge deck. Therefore, the attention is paid to cable-stayed beam and quite a few studies are carried out [14, 15]. Fujino et al. [16] established a cable-beam model considering three degrees of freedom (DOFs) and proposed the concepts of global mode and local mode. Meanwhile, the 1:1:2 internal resonance among different modes were observed experimentally. Gattulli and co-workers [17–19] used a localization factor to recognize the global mode and local mode and the nonlinear behaviors of the cable-stayed beam were analyzed in detail. They found that for a highly tensioned cable-stayed beam, the global modes exhibit softening characteristics, while the local modes show hardening behaviors.

The researches mentioned above reveal that the cable-stayed beam is prone to vibration under the action of ambient excitation [20]. To suppress the vibration, a damper is usually installed near the lower end of the cable. The simplest model to describe the fact is a taut cable with a viscous damper. Krenk [21] studied the model by expressing the solutions with damped complex-valued modes. In this way, a simple iterative solution of the characteristic equation for all complex eigenfrequencies was proposed. Thereafter, Krenk and Nielsen [22] considered a shallow cable with a viscous damper by taking the sag of the cable into account. Main and Jones [23] investigated the complex eigenvalue problem of a taut cable with a linear damper. Different from the work of Krenk, the solutions were obtained without approximation. In addition, Main and Jones [24] also considered a taut cable with a nonlinear damper, in which they pointed out that the nonlinear damper might have a potential superiority in terms of vibration suppression compared with the linear damper.

Using the harmonic balance method, Xu and Yu [25, 26] explored the nonlinear behaviors of inclined sag cables with oil dampers. The results show that the oil dampers can effectively suppress both the in-plane vibration and non-planar vibration of the cable. However, the suppression effectiveness of the viscous damper is limited because the damper is usually placed at a distance of 2–5% from the lower end of the cable. To overcome this geometric limitation, it is recommended to install a TMD on the cable, i.e., cable-TMD model. Cai et al. [27–29] conducted a detailed analysis on the model. The rule of damping redistribution to each mode of the cable was studied. The results show that various parameters have a large impact on the modal damping of the system. Recently, Su et al. [30] investigated the one-to-one internal resonance between the cable and TMD by considering the vibration of the TMD. The energy transfer between the cable and TMD was revealed.

Nevertheless, the above studies assume that the lower end of the cable is fixed and the motion of the bridge deck is not taken into account. In practical engineering, the bridge deck will inevitably be involved in the movement of the cable and damper, thus affecting the suppression effect of the damper. Luo et al. [31] analyzed the effects of different parameters on the modal damping of a cable-damper system under the excitation of bridge deck. Liang et al. [32] concluded that as the span of the cable-stayed bridge increases, the vibration of the beam became one of the main factors affecting the suppression effectiveness of the damper on the cable. However, these studies are mainly concerned with complex eigenvalue problem of the system. To better understand the vibration suppression, it is important to study the nonlinear characteristics of the structures [33]. Actually, as a member installed on the cable, the damper is necessarily involved in the coupled interaction between the cable and beam. Nevertheless, the researches that the damper participates as a DOF in the coupled vibration of the cable-beam model have hardly been seen. Moreover, will the damper take part in the energy transfer between the beam and cable while consuming energy? Relevant studies have never been reported. On the other hand, the cable-cantilever beam model is suitable for the construction state of the cable-stayed bridge, but it is more reasonable to use the cable-stayed beam model to simulate the completion state of the cable-stayed bridge.

Based on the above research background, the motivation of this work is to explore the dynamic behaviors of the beam, cable and TMD and their energy transfer in the system of a cable-stayed beam with a TMD. The one-to-one-to-one internal resonance among the beam, cable and TMD is considered while the external primary resonance occurs. The novelty here stays in considering a fully coupled and internally resonant nonlinear system, namely the cable-beam-TMD model (Case 1), such to allow the description of energy transfer among the beam, cable and TMD. Meanwhile, the cable-beam-TMD model without the vibration of the TMD (Case 2), which corresponds to considering only energy consumption, is also examined. The two cases are compared with each other to reveal the role of the TMD in not only energy consumption but also energy transfer.

The remainder of the paper is organized as follows. In Sect. 2, the cable-beam-TMD model is presented. The corresponding ODEs are derived and solved by perturbation technique. Section 3 is devoted to numerical results and discussions. Conclusions are given in Sect. 4.

2 Governing equations and perturbation technique

The problem under consideration is depicted in Fig. 1. In the figure, two Cartesian coordinates, namely, $s^*o^*y^*$ and $x^*o_1^*y_1^*$, are established to describe the motion of the cable and beam. The beam is subjected to a harmonic loading $F_1^*(s^*)\cos\Omega^*t$, which can excite only the first mode of the beam. $F_1^*(s^*)$ describes the spatial distribution of the harmonic load and Ω^* is the frequency. The length of the beam and cable is L and l_c, respectively. $l_1^*(l_2^*)$ is the distance between the TMD and upper (lower) end of the cable. θ is the acute angle between axes of the cable and beam. The cable and beam are coupled with each other at the node s_1^*. M_d^*, K_d^* and C_d^* represent the mass, spring stiffness and damping coefficient of the TMD, respectively. For the sake of simplicity, the following assumptions are made: (a) the ratio of the sag to length of the cable is small; (b) the axial vibration of the beam and the longitudinal inertia force of the cable are negligible; (c) ignore the contribution of the tension of the cable to the axial force of the beam; (d) the shear strain, torsional and shear rigidities of the beam are negligible; (e) the vibration amplitude of the beam is much smaller than that of the cable. Hence, the effect of the transverse movement of the beam on the cable is assumed to be vertical dragging.

Based on the above assumptions, the equations of motion of the beam [14], cable and TMD can be derived according to the extended Hamilton's principle [34], i.e.

$$\rho_b A_b \ddot{v}_b^* + \mu_b^* \dot{v}_b^* + E_b I_b v_b''''^*$$
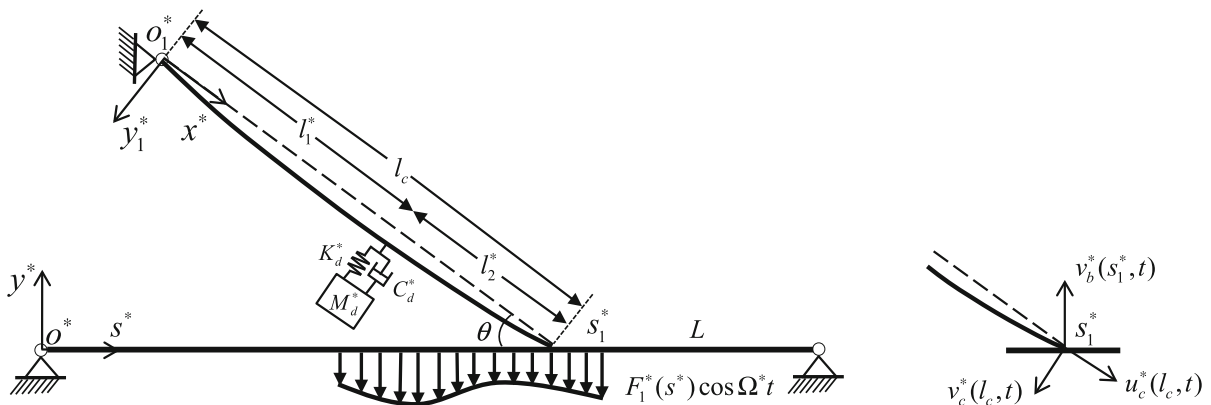$$- E_b A_b \left(\frac{1}{L} \int_0^L \frac{1}{2} v_b'^{2*} \mathrm{d}s^* \right) v_b''^* = p_b^*(s^*, t) \quad (1)$$

Fig. 1 A cable-stayed beam model with a TMD: cable-beam-TMD model

$$\rho_c A_c \ddot{v}_c^* + \mu_c^* \dot{v}_c^* - \left[H_c v_c''^* + E_c A_c \left(v_c''^* + y_c''^* \right) e_c^*(t) \right] = -f^*(t)\delta(x^* - l_1^*)$$

(2)

$$K_d^*[v_c^*(l_1^*, t) - v_d^*] + C_d^*[\dot{v}_c^*(l_1^*, t) - \dot{v}_d^*] - M_d^* \ddot{v}_d^* = 0$$

(3)

where the subscripts b, c and d denote beam, cable and TMD, respectively. ρ, A, μ^*, E, and I are mass per unit volume, cross-sectional area, damping coefficient per unit length, Young's modulus and second moment of area, respectively. H_c is the initial force of the cable. v_b^* and v_c^* are planar transverse displacements of the beam and cable, respectively. v_d^* is the displacement of the TMD along the y_1^* axis. The dot and primes represent differentiations with respect to time t and local abscissae x^* and s^*, respectively. $\delta()$ denotes Kronecker delta function. $e_c^*(t)$ is the extensional strain in the cable motion and is defined as

$$e_c^*(t) = \frac{u_c^*(l_c, t)}{l_c} + \frac{1}{l_c} \int_0^{l_c} \left(y_c'^* v_c'^* + \frac{1}{2} v_c'^{2*} \right) dx^*$$

(4)

where u_c^* is the axial displacement of the cable. y_c^* is the static equilibrium configuration of the cable, which is described through a parabola according to assumption (a), namely

$$y_c^*(x^*) = 4d_c^* \left[\frac{x^*}{l_c} - \left(\frac{x^*}{l_c} \right)^2 \right]$$

(5)

where d_c^* is the cable sag and is determined by $d_c^* = \frac{\rho_c A_c \varsigma l_c^2 \cos\theta}{8H_c}$ (ς is the gravity acceleration).

According to Fig. 1, the boundary conditions of the system can be written as follows

$$v_b^*(0, t) = v_b^*(L, t) = 0$$

(6)

$$v_b''^*(0, t) = v_b''^*(L, t) = 0$$

(7)

$$v_c^*(0, t) = 0$$

(8)

The displacement relationship at the node s_1^* (see Fig. 1) is

$$u_c^*(l_c, t) = -v_b^*(s_1^*, t)\sin\theta$$

(9)

Substituting Eqs. (9) into (4) may yield

$$e_c^*(t) = -\frac{v_b^*(s_1^*, t)\sin\theta}{l_c} + \frac{1}{l_c} \int_0^{l_c} \left(y_c'^* v_c'^* + \frac{1}{2} v_c'^{2*} \right) dx^*$$

(10)

Additionally, in Fig. 1, $p_b^*(s^*, t)$ is the total load acting on the beam, which contains two parts. The first part is the force contributed by the cable. The second part is the external harmonic loading. Hence, the expression of $p_b^*(s^*, t)$ is

$$p_b^*(s^*, t) = \delta(s^* - s_1^*)E_c A_c e_c^*(t)\sin\theta + F_1^*(s^*)\cos\Omega^* t$$

(11)

In Eq. (2), $f^*(t)$ is the force applied to the cable by the TMD and its expression is

$$f^*(t) = K_d^*[v_c^*(l_1^*, t) - v_d^*] + C_d^*[\dot{v}_c^*(l_1^*, t) - \dot{v}_d^*]$$

(12)

In the following, several non-dimensional quantities are introduced to obtain the non-dimensional forms of the equations of motion of the system.

$$x = \tfrac{x^*}{l_c}, \quad \tau = \omega_0 t, \quad y_c = \tfrac{y_c^*}{l_c}, \quad d_c = \tfrac{d_c^*}{l_c}, \quad l_1 = \tfrac{l_1^*}{l_c}, \quad l_2 = \tfrac{l_2^*}{l_c},$$
$$v_c = \tfrac{v_c^*}{l_c}, \quad \gamma_c = \tfrac{L}{l_c}, \quad \mu_c = \tfrac{\mu_c^*}{\rho_c A_c \omega_0}, \quad \lambda_c = \tfrac{E_c A_c}{H_c}, \quad \beta_c^2 = \tfrac{\rho_c A_c \omega_0^2 l_c^2}{H_c},$$
$$f(t) = \tfrac{f^*(t)}{\rho_c A_c \omega_0^2 l_c}, \quad \psi_c = \tfrac{E_c A_c}{\rho_b A_b \omega_0^2 L}, \quad v_b = \tfrac{v_b^*}{L}, \quad s = \tfrac{s^*}{L},$$
$$\mu_b = \tfrac{\mu_b^*}{\rho_b A_b \omega_0}, \quad \Omega = \tfrac{\Omega^*}{\omega_0}, \quad \beta_b^4 = \tfrac{\rho_b A_b \omega_0^2 L^4}{E_b I_b}, \quad p_b = \tfrac{p_b^*}{\rho_b A_b \omega_0^2 L},$$
$$F_1(s) = \tfrac{F_1^*(s^*)}{\rho_b A_b \omega_0^2 L}, \quad \eta_b = \tfrac{A_b L^2}{I_b}, \quad \omega_0 = 1.0 rad \cdot s^{-1}, \quad v_d = \tfrac{v_d^*}{l_c},$$
$$M_d = \tfrac{M_d^*}{\rho_c A_c}, \quad K_d = \tfrac{K_d^*}{\rho_c A_c \omega_0^2}, \quad C_d = \tfrac{C_d^*}{\rho_c A_c \omega_0}, \quad \omega_d^2 = \tfrac{K_d}{M_d},$$
$$\xi_d = \tfrac{C_d}{2M_d \omega_d}.$$

In this way, Eqs. (1)–(3), (5) and (10) are rewritten as

$$\ddot{v}_b + \mu_b \dot{v}_b + \frac{1}{\beta_b^4} v_b'''' - \frac{\eta_b}{\beta_b^4} \left(\int_0^1 \frac{1}{2} v_b'^2 ds \right) v_b'' = \delta(s - s_1)\psi_c e_c(\tau)\sin\theta + F_1(s)\cos\Omega\tau$$

(13)

$$\ddot{v}_c + \mu_c \dot{v}_c - \frac{1}{\beta_c^2} \left[v_c'' + \lambda_c (v_c'' + y_c'') e_c(\tau) \right] = -(K_d[v_c(l_1, \tau) - v_d] + C_d[\dot{v}_c(l_1, \tau) - \dot{v}_d])\delta(x - l_1)$$

(14)

$$\omega_d^2[v_c(l_1, \tau) - v_d] + 2\xi_d \omega_d[\dot{v}_c(l_1, \tau) - \dot{v}_d] - \ddot{v}_d = 0$$

(15)

$$y_c(x) = 4d_c x(1 - x)$$

(16)

$$e_c(\tau) = -\gamma_c v_b(s_1, \tau) \sin\theta + \int_0^1 \left(y_c' v_c' + \frac{1}{2} v_c'^2\right) dx \tag{17}$$

A discrete model of the continuum system is obtained by assuming the planar transverse displacement of the beam to be the following form

$$v_b(s, \tau) = \phi_b(s) g(\tau) \tag{18}$$

Nevertheless, following assumption (e), the non-dimensional expression of the planar transverse displacement of the cable is

$$v_c(x, \tau) = -\gamma_c v_b(s_1, \tau) x \cos(\theta) + \phi_c(x) q_c(\tau) \tag{19}$$

where the first term at the right hand reflects the dragging effect of the beam on the cable and the second term denotes the pure modal displacement of the cable. Moreover, $g(\tau)$ and $q_c(\tau)$ are generalized coordinates. $\phi_b(s)$ and $\phi_c(x)$ are the shape functions. In this paper, the sine function $\sin(\pi s)$ is utilized for $\phi_b(s)$. With regard to $\phi_c(x)$, the reference [35] verifies that the change of the mode shapes caused by TMD will tend quickly to zero as the mass ratio of TMD to cable tends to zero. For a small value of the ratio (the ratio in this paper is 5%), such a difference is ignorable and mode shapes of the cable without the TMD could be considered to be a good approximation of the mode shapes of the cable with the TMD. Hence, the sine function $\sin(\pi x)$ is also adopted for $\phi_c(x)$, which is used in many previous studies [30, 36–38]. Substituting Eqs. (18) and (19) into Eqs. (13) and (14) and using the Galerkin's method, the following ODEs can be obtained

$$\ddot{g} + \mu_b \dot{g} + b_{11} g + b_{12} g^2 + b_{13} g^3 + b_{14} q_c + b_{15} g q_c$$
$$\quad + b_{16} q_c^2 + b_{17} \cos(\Omega\tau)$$
$$= 0 \tag{20}$$

$$\ddot{q}_c + b_{21} q_c + b_{22} \dot{q}_c + b_{23} \dot{g} + b_{24} \ddot{g} + b_{25} g + b_{26} g^2$$
$$\quad + b_{27} g q_c + b_{28} q_c^2 + b_{29} g^2 q_c + b_{210} g q_c^2 + b_{211} q_c^3$$
$$\quad + b_{212} v_d + b_{213} \dot{v}_d$$
$$= 0 \tag{21}$$

Similarly, substituting Eqs. (18) and (19) into Eq. (15), the ODE of the TMD can be derived

$$\ddot{v}_d + \omega_d^2 v_d + b_{31} \dot{v}_d + b_{32} g + b_{33} q_c + b_{34} \dot{g} + b_{35} \dot{q}_c$$
$$= 0 \tag{22}$$

In Eqs. (20)–(22), b_{ij} ($i = 1, 2, 3, j = 1, 2, 3,...,13$) are Galerkin integral coefficients and they are reported in Appendix A. It can be seen that there exists terms related to the beam in Eq. (22). This will affect the nonlinear characteristics of the TMD, which in turn has an influence on the nonlinear behaviors of the beam and cable.

In the following, the MTS method is utilized to solve the ODEs. To this end, a small bookkeeping parameter ε and new independent time variables $T_n = \varepsilon^n \tau (n = 0, 1, 2)$ are introduced. In this way, the derivatives with respect to time τ can be written as

$$\frac{d}{d\tau} = \frac{\partial}{\partial T_0} \frac{dT_0}{d\tau} + \frac{\partial}{\partial T_1} \frac{dT_1}{d\tau} + \frac{\partial}{\partial T_2} \frac{dT_2}{d\tau} + \cdots$$
$$= D_0^1 + \varepsilon D_1^1 + \varepsilon^2 D_2^1 + \cdots$$
$$\frac{d^2}{d\tau^2} = (D_0^1 + \varepsilon D_1^1 + \varepsilon^2 D_2^1 + \cdots)^2$$
$$= D_0^2 + 2\varepsilon D_0^1 D_1^1 + 2\varepsilon^2 D_0^1 D_2^1 + \cdots \tag{23}$$

where D_n^r is a differential operator and it is defined as $D_n^r = \partial^r / \partial T_n$ ($r = 1,2$ and $n = 0, 1, 2$). In order to balance the damping, excitation and nonlinear terms, the coefficients in Eqs. (20)–(22) are reordered. Correspondingly, Eqs. (20)–(22) are rewritten as

$$\ddot{g} + \varepsilon^2 \mu_b \dot{g} + \omega_b^2 g + \varepsilon b_{12} g^2 + \varepsilon^2 b_{13} g^3 + \varepsilon b_{14} q_c$$
$$\quad + \varepsilon b_{15} g q_c + \varepsilon b_{16} q_c^2 + \varepsilon^2 b_{17} \cos(\Omega\tau)$$
$$= 0 \tag{24}$$

$$\ddot{q}_c + \omega_c^2 q_c + \varepsilon^2 b_{22} \dot{q}_c + \varepsilon^2 b_{23} \dot{g} + \varepsilon^2 b_{24} \ddot{g} + \varepsilon b_{25} g$$
$$\quad + \varepsilon b_{26} g^2 + \varepsilon b_{27} g q_c + \varepsilon b_{28} q_c^2 + \varepsilon^2 b_{29} g^2 q_c$$
$$\quad + \varepsilon^2 b_{210} g q_c^2 + \varepsilon^2 b_{211} q_c^3 + \varepsilon b_{212} v_d + \varepsilon^2 b_{213} \dot{v}_d = 0 \tag{25}$$

$$\ddot{v}_d + \omega_d^2 v_d + \varepsilon^2 b_{31} \dot{v}_d + \varepsilon b_{32} g + \varepsilon b_{33} q_c + \varepsilon^2 b_{34} \dot{g}$$
$$\quad + \varepsilon^2 b_{35} \dot{q}_c$$
$$= 0 \tag{26}$$

where $\omega_b^2 = b_{11}$ and $\omega_c^2 = b_{21}$ are natural frequencies of the beam and cable, respectively. Following the principle of MTS method, a second order approximation is sought and the solutions for g, q_c and v_d are uniformly expanded in power series of ε, i.e.

$$g = \sum_{i=1}^{3} \varepsilon^{i-1} g_i(T_0, T_1, T_2) + O(\varepsilon^3)$$

$$q_c = \sum_{i=1}^{3} \varepsilon^{i-1} q_{ci}(T_0, T_1, T_2) + O(\varepsilon^3) \tag{27}$$

$$v_d = \sum_{i=1}^{3} \varepsilon^{i-1} v_{di}(T_0, T_1, T_2) + O(\varepsilon^3)$$

Substituting Eq. (27) into Eqs. (24)–(26) and equating the terms of like order in ε lead to order ε^0,

$$\begin{aligned}
(D_0^2 + \omega_b^2)g &= 0 \\
(D_0^2 + \omega_c^2)q_{c1} &= 0 \\
(D_0^2 + \omega_d^2)v_{d1} &= 0
\end{aligned} \tag{28}$$

order ε^1,

$$\begin{aligned}
(D_0^2 + \omega_b^2)g_2 &= -(b_{12}g_1^2 + b_{14}q_1 + b_{15}g_1q_{c1} + b_{16}q_{c1}^2 + 2D_0^1 D_1^1 g_1) \\
(D_0^2 + \omega_c^2)q_{c2} &= -(b_{25}g_1 + b_{26}g_1^2 + b_{27}g_1q_{c1} + b_{26}q_{c1}^2 \\
&\quad + b_{212}v_{d1} + 2D_0^1 D_1^1 q_{c1}) \\
(D_0^2 + \omega_d^2)v_{d2} &= -(b_{32}g_1 + b_{33}q_{c1} + 2D_0^1 D_1^1 v_{d1})
\end{aligned} \tag{29}$$

order ε^2,

$$\begin{aligned}
(D_0^2 + \omega_b^2)g_3 &= -b_{17}\cos(\Omega T_0) - 2b_{12}g_1 g_2 - b_{13}g_1^3 \\
&\quad - b_{14}q_{c2} - b_{15}g_2q_{c1} - b_{15}g_1q_{c2} - 2b_{16}q_{c1}q_{c2} - D_1^2 g_1 \\
&\quad - \mu_b D_0^1 g_1 - 2D_0^1 D_2^1 g_1 - 2D_0^1 D_1^1 g_2 \\
(D_0^2 + \omega_c^2)q_{c3} &= -(b_{25}g_2 + 2b_{26}g_1 g_2 + b_{27}g_2 q_{c1} \\
&\quad + b_{27}g_1 q_{c2} + 2b_{28}q_{c1}q_{c2} + b_{29}g_1^2 q_{c1} \\
&\quad + b_{210}g_1 q_{c1}^2 + b_{211}q_{c1}^3 + b_{212}v_{d2} + D_1^2 q_{c1} + b_{23}D_0^1 g_1 \\
&\quad + b_{22}D_0^1 q_{c1} + b_{213}D_0^1 v_{d1} + 2D_0^1 D_2^1 q_{c1} \\
&\quad + 2D_1^1 D_1^1 q_{c2} + b_{24}D_0^2 g_1) \\
(D_0^2 + \omega_d^2)v_{d3} &= -(b_{32}g_2 + b_{33}q_{c2} + D_1^2 v_{d1} + b_{34}D_0^1 g_1 \\
&\quad + b_{35}D_0^1 q_{c1} + b_{31}D_0^1 v_{d1} + 2D_0^1 D_2^1 v_{d1} \\
&\quad + 2D_0^1 D_1^1 v_{d2})
\end{aligned} \tag{30}$$

The solutions of system (28) are

$$g_1 = A_1(T_1, T_2)\exp(i\omega_b T_0) + cc \tag{31}$$

$$q_{c1} = A_2(T_1, T_2)\exp(i\omega_c T_0) + cc \tag{32}$$

$$v_{d1} = A_3(T_1, T_2)\exp(i\omega_d T_0) + cc \tag{33}$$

where $A_m(T_1, T_2)(m = 1,2,3)$ denote complex amplitudes which will be determined by solving the higher order Eqs. (29) and (30). cc represent the complex conjugates of the preceding terms and

$i = \sqrt{-1}$. Substituting Eqs. (31)–(33) into Eq. (29) yields

$$\begin{aligned}
(D_0^2 + \omega_b^2)g_2 &= -b_{12}\exp(2iT_0\omega_b)A_1^2 - b_{14}\exp(iT_0\omega_c)A_2 \\
&\quad - b_{15}\exp(iT_0(\omega_b + \omega_c))A_1A_2 - b_{16}\exp(2iT_0\omega_c)A_2^2 \\
&\quad - b_{15}\exp(iT_0(\omega_b - \omega_c))A_1B_2 - 2i\omega_b\exp(iT_0\omega_b)D_1^1 A_1 \\
&\quad - b_{12}A_1B_1 - b_{16}A_2B_2 + cc
\end{aligned} \tag{34}$$

$$\begin{aligned}
(D_0^2 + \omega_c^2)q_{c2} &= -b_{25}\exp(iT_0\omega_b)A_1 - b_{26}\exp(2iT_0\omega_b)A_1^2 \\
&\quad - b_{27}\exp(iT_0(\omega_b + \omega_c))A_1A_2 - b_{28}\exp(2iT_0\omega_c)A_2^2 \\
&\quad - b_{212}\exp(iT_0\omega_d)A_3 - b_{27}\exp(iT_0(\omega_b - \omega_c)) \\
&\quad A_1B_2 - 2i\omega_c\exp(iT_0\omega_c)D_1^1 A_2 - b_{26}A_1B_1 \\
&\quad - b_{28}A_2B_2 + cc
\end{aligned} \tag{35}$$

$$\begin{aligned}
(D_0^2 + \omega_d^2)v_{d2} &= -b_{32}\exp(iT_0\omega_b)A_1 \\
&\quad - b_{33}\exp(iT_0\omega_c)A_2 \\
&\quad - 2i\omega_d\exp(iT_0\omega_d)D_1^1 A_3 + cc
\end{aligned} \tag{36}$$

where $B_m(T_1, T_2)$ is the complex conjugate of $A_m(T_1, T_2)$ and (T_1, T_2) has been dropped for simplicity. Considering one-to-one-to-one internal resonance of the system when external primary resonance of the beam occurs, the nearness of the frequencies can be described by introducing the following relationships

$$\Omega = \omega_b + \varepsilon^2 \sigma_1, \omega_b = \omega_c + \varepsilon\sigma_2, \omega_d = \omega_c + \varepsilon\sigma_3 \tag{37}$$

where σ_1 is external detuning parameter and σ_2 and σ_3 are internal detuning parameters. Substituting Eq. (37) into Eqs. (34)–(36) and eliminating the corresponding secular terms (letting the secular terms equal to zero), the 1st-order solvability condition can be obtained as follows

$$ib_{14}\exp(-iT_1\sigma_2)A_2 - 2\omega_b D_1^1 A_1 = 0 \tag{38}$$

$$ib_{25}\exp(iT_1\sigma_2)A_1 + ib_{212}\exp(iT_1\sigma_3)A_3 - 2\omega_c D_1^1 A_2 = 0 \tag{39}$$

$$\begin{aligned}
&ib_{32}\exp(iT_1(\sigma_2 - \sigma_3))A_1 + ib_{33}\exp(-iT_1\sigma_3)A_2 \\
&- 2\omega_d D_1^1 A_3 = 0
\end{aligned} \tag{40}$$

Meanwhile, the solutions for g_2, q_{c2} and v_{d2} are obtained after eliminating the secular terms. The resulting solutions and Eqs. (31)–(33) are substituted into Eq. (30) and in the final, the following equations can be derived

$$(D_0^2 + \omega_b^2)g_3 = -\frac{1}{2}b_{17}\exp(iT_0\Omega) - i\mu_b\omega_b\exp(iT_0\omega_b)A_1$$
$$+ \exp(iT_0\omega_b)\Gamma_{14}A_1^2B_1 + \exp(iT_0\omega_c)\Gamma_{15}A_1A_2B_1$$
$$+ \exp(-iT_0(\omega_b - 2\omega_c))\Gamma_{16}A_2^2B_1$$
$$+ \exp(iT_0(2\omega_b - \omega_c))\Gamma_{17}A_1^2B_2 + \exp(iT_0\omega_b)\Gamma_{18}A_1A_2B_2$$
$$+ \exp(iT_0\omega_c)\Gamma_{19}A_2^2B_2 - 2i\omega_b\exp(iT_0\omega_b)D_2^1A_1$$
$$- \exp(iT_0\omega_b)D_1^2A_1 + NST_1 + cc$$

$$(41)$$

$$(D_0^2 + \omega_c^2)q_{c3} = -ib_{23}\omega_b\exp(iT_0\omega_b)A_1 + b_{24}\omega_b^2\exp(iT_0\omega_b)A_1$$
$$- ib_{22}\omega_c\exp(iT_0\omega_c)A_2 - ib_{213}\omega_d\exp(iT_0\omega_d)A_3$$
$$+ \exp(iT_0\omega_b)\Gamma_{24}A_1^2B_1 + \exp(iT_0\omega_c)\Gamma_{25}A_1A_2B_1$$
$$+ \exp(-iT_0(\omega_b - 2\omega_c))\Gamma_{26}A_2^2B_1$$
$$+ \exp(iT_0(2\omega_b - \omega_c))\Gamma_{27}A_1^2B_2 + \exp(iT_0\omega_b)\Gamma_{28}A_1A_2B_2$$
$$+ \exp(iT_0\omega_c)\Gamma_{29}A_2^2B_2$$
$$- 2i\omega_c\exp(iT_0\omega_c)D_2^1A_2 - \exp(iT_0\omega_c)D_1^2A_2 + NST_2 + cc$$

$$(42)$$

$$(D_0^2 + \omega_d^2)v_{d3} = -ib_{34}\omega_b\exp(iT_0\omega_b)A_1$$
$$- ib_{35}\omega_c\exp(iT_0\omega_c)A_2$$
$$- ib_{31}\omega_d\exp(iT_0\omega_d)A_3 - 2i\omega_d$$
$$\exp(iT_0\omega_d)D_2^1A_3$$
$$- \exp(iT_0\omega_d)D_1^2A_3 + NST_3 + cc$$

$$(43)$$

According to Eqs. (38)–(40), the expressions of $D_1^1A_m$ and $D_1^2A_m$ can be solved. Substituting the results into Eqs. (41)–(43) yields

$$(D_0^2 + \omega_b^2)g_3 = -\frac{1}{2}b_{17}\exp(iT_0\Omega) - i\mu_b\omega_b\exp(iT_0\omega_b)A_1$$
$$+ \exp(iT_0\omega_b)\Gamma_{11}A_1 + \exp(iT_0\omega_c)\Gamma_{12}A_2$$
$$+ \exp(iT_0\omega_d)\Gamma_{13}A_3 + \exp(iT_0\omega_b)\Gamma_{14}A_1^2B_1$$
$$+ \exp(iT_0\omega_c)\Gamma_{15}A_1A_2B_1$$
$$+ \exp(-iT_0(\omega_b - 2\omega_c))\Gamma_{16}A_2^2B_1$$
$$+ \exp(iT_0(2\omega_b - \omega_c))\Gamma_{17}A_1^2B_2 + \exp(iT_0\omega_b)\Gamma_{18}A_1A_2B_2$$
$$+ \exp(iT_0\omega_c)\Gamma_{19}A_2^2B_2 - 2i\omega_b\exp(iT_0\omega_b)D_2^1A_1 + NST_1 + cc$$

$$(44)$$

$$(D_0^2 + \omega_c^2)q_{c3} = -ib_{23}\omega_b\exp(iT_0\omega_b)A_1 - ib_{22}\omega_c\exp(iT_0\omega_c)A_2$$
$$- ib_{213}\omega_d\exp(iT_0\omega_d)A_3 + \exp(iT_0\omega_b)\Gamma_{21}A_1$$
$$+ \exp(iT_0\omega_c)\Gamma_{22}A_2 + \exp(iT_0\omega_d)\Gamma_{23}A_3$$
$$+ \exp(iT_0\omega_b)\Gamma_{24}A_1^2B_1 + \exp(iT_0\omega_c)\Gamma_{25}A_1A_2B_1$$
$$+ \exp(-iT_0(\omega_b - 2\omega_c))\Gamma_{26}A_2^2B_1$$
$$+ \exp(iT_0(2\omega_b - \omega_c))\Gamma_{27}A_1^2B_2 + \exp(iT_0\omega_b)\Gamma_{28}A_1A_2B_2$$
$$+ \exp(iT_0\omega_c)\Gamma_{29}A_2^2B_2 - 2i\omega_c\exp(iT_0\omega_c)D_2^1A_2$$
$$+ NST_2 + cc$$

$$(45)$$

$$(D_0^2 + \omega_d^2)v_{d3} = -ib_{34}\omega_b\exp(iT_0\omega_b)A_1$$
$$- ib_{35}\omega_c\exp(iT_0\omega_c)A_2$$
$$- ib_{31}\omega_d\exp(iT_0\omega_d)A_3 + \exp(iT_0\omega_b)\Gamma_{31}A_1$$
$$+ \exp(iT_0\omega_c)\Gamma_{32}A_2 + \exp(iT_0\omega_d)\Gamma_{33}A_3$$
$$- 2i\omega_d\exp(iT_0\omega_d)D_2^1A_3 + NST_3 + cc$$

$$(46)$$

where NST_m denote non-secular terms. The coefficients $\Gamma_{ij}(i = 1,2,3, j = 1,2,3,…,9)$ are reported in Appendix B. Eliminating the secular terms in Eqs. (44)–(46) may yield the 2nd-order solvability, namely

$$-\frac{1}{2}b_{17}\exp(iT_0\Omega) - i\mu_b\omega_b\exp(iT_0\omega_b)A_1 + \exp(iT_0\omega_b)\Gamma_{11}A_1$$
$$+ \exp(iT_0\omega_c)\Gamma_{12}A_2 + \exp(iT_0\omega_d)\Gamma_{13}A_3$$
$$+ \exp(iT_0\omega_b)\Gamma_{14}A_1^2B_1 + \exp(iT_0\omega_c)\Gamma_{15}A_1A_2B_1$$
$$+ \exp(-iT_0(\omega_b - 2\omega_c))\Gamma_{16}A_2^2B_1 + \exp(iT_0(2\omega_b - \omega_c))\Gamma_{17}A_1^2B_2$$
$$+ \exp(iT_0\omega_b)\Gamma_{18}A_1A_2B_2 + \exp(iT_0\omega_c)\Gamma_{19}A_2^2B_2$$
$$- 2i\omega_b\exp(iT_0\omega_b)D_2^1A_1 = 0$$

$$(47)$$

$$-ib_{23}\omega_b\exp(iT_0\omega_b)A_1 - ib_{22}\omega_c\exp(iT_0\omega_c)A_2$$
$$- ib_{213}\omega_d\exp(iT_0\omega_d)A_3 + \exp(iT_0\omega_b)\Gamma_{21}A_1$$
$$+ \exp(iT_0\omega_c)\Gamma_{22}A_2$$
$$+ \exp(iT_0\omega_d)\Gamma_{23}A_3 + \exp(iT_0\omega_b)\Gamma_{24}A_1^2B_1$$
$$+ \exp(iT_0\omega_c)\Gamma_{25}A_1A_2B_1 + \exp(-iT_0(\omega_b - 2\omega_c))\Gamma_{26}A_2^2B_1$$
$$+ \exp(iT_0(2\omega_b - \omega_c))\Gamma_{27}A_1^2B_2 + \exp(iT_0\omega_b)\Gamma_{28}A_1A_2B_2$$
$$+ \exp(iT_0\omega_c)\Gamma_{29}A_2^2B_2 - 2i\omega_c\exp(iT_0\omega_c)D_2^1A_2 = 0$$

$$(48)$$

$$-ib_{34}\omega_b\exp(iT_0\omega_b)A_1 - ib_{35}\omega_c\exp(iT_0\omega_c)A_2$$
$$- ib_{31}\omega_d\exp(iT_0\omega_d)A_3 + \exp(iT_0\omega_b)\Gamma_{31}A_1$$
$$+ \exp(iT_0\omega_c)\Gamma_{32}A_2 + \exp(iT_0\omega_d)\Gamma_{33}A_3$$
$$- 2i\omega_d\exp(iT_0\omega_d)D_2^1A_3 = 0$$

$$(49)$$

In order to solve Eqs. (47)–(49), the following polar transformation is introduced

$$A_m(T_1, T_2) = \frac{1}{2}a_m(T_1, T_2)\exp(i\Phi_m(T_1, T_2)) \quad (50)$$

where a_m and Φ_m are the amplitude and phase angle of A_m. Substituting Eq. (50) into the 1st-order and 2nd-order solvability conditions and separating the real and imaginary parts, respectively, the autonomous modulation equations can be obtained as follows

$$D_1^1 a_1 = \frac{b_{14} a_2 \sin \alpha_2}{2\omega_b} \tag{51}$$

$$D_1^1 \alpha_1 = -\frac{b_{14} a_2 \cos \alpha_2}{2\omega_b a_1} \tag{52}$$

$$D_1^1 a_2 = -\frac{b_{25} a_1 \sin \alpha_2}{2\omega_c} - \frac{b_{212} a_3 \sin \alpha_3}{2\omega_c} \tag{53}$$

$$D_1^1 \alpha_2 = \sigma_2 - \frac{b_{25} a_1 \cos \alpha_2}{2\omega_c a_2} + \frac{b_{14} a_2 \cos \alpha_2}{2\omega_b a_1} - \frac{b_{212} a_3 \cos \alpha_3}{2\omega_c a_2} \tag{54}$$

$$D_1^1 a_3 = -\frac{b_{32} a_1 \sin(\alpha_2 - \alpha_3)}{2\omega_d} + \frac{b_{33} a_2 \sin \alpha_3}{2\omega_d} \tag{55}$$

$$D_1^1 \alpha_3 = \sigma_3 - \frac{b_{25} a_1 \cos \alpha_2}{2\omega_c a_2} + \frac{b_{32} a_1 \cos(\alpha_2 - \alpha_3)}{2\omega_d a_3} + \frac{b_{33} a_2 \cos \alpha_3}{2\omega_d a_3} - \frac{b_{212} a_3 \cos \alpha_3}{2\omega_c a_2} \tag{56}$$

$$D_2^1 a_1 = -\frac{\mu_b a_1}{2} - \frac{b_{17} \sin \alpha_1}{2\omega_b} - \frac{\Gamma_{12} a_2 \sin \alpha_2}{2\omega_b} + \frac{(\Gamma_{17} - \Gamma_{15}) a_1^2 a_2 \sin \alpha_2}{8\omega_b} - \frac{\Gamma_{19} a_2^3 \sin \alpha_2}{8\omega_b} - \frac{\Gamma_{16} a_2^2 a_1 \sin 2\alpha_2}{8\omega_b} - \frac{\Gamma_{13} a_3 \sin(\alpha_2 - \alpha_3)}{2\omega_b} \tag{57}$$

$$D_2^1 \alpha_1 = \sigma_1 + \frac{\Gamma_{11}}{2\omega_b} + \frac{\Gamma_{14} a_1^2}{8\omega_b} + \frac{\Gamma_{18} a_2^2}{8\omega_b} - \frac{b_{17} \cos \alpha_1}{2\omega_b a_1} + \frac{\Gamma_{12} a_2 \cos \alpha_2}{2\omega_b a_1} + \frac{(\Gamma_{15} + \Gamma_{17}) a_1 a_2 \cos \alpha_2}{8\omega_b} + \frac{\Gamma_{19} a_2^3 \cos \alpha_2}{8\omega_b a_1} + \frac{\Gamma_{16} a_2^2 \cos 2\alpha_2}{8\omega_b} + \frac{\Gamma_{13} a_3 \cos(\alpha_2 - \alpha_3)}{2\omega_b a_1} \tag{58}$$

$$D_2^1 a_2 = -\frac{b_{22} a_2}{2} - \frac{b_{23} \omega_b a_1 \cos \alpha_2}{2\omega_c} - \frac{b_{213} \omega_d a_3 \cos \alpha_3}{2\omega_c} + \frac{\Gamma_{21} a_1 \sin \alpha_2}{2\omega_c} + \frac{\Gamma_{24} a_1^3 \sin \alpha_2}{8\omega_c} + \frac{(\Gamma_{28} - \Gamma_{26}) a_1 a_2^2 \sin \alpha_2}{8\omega_c} + \frac{\Gamma_{27} a_2 a_1^2 \sin 2\alpha_2}{8\omega_c} + \frac{\Gamma_{23} a_3 \sin \alpha_3}{2\omega_c} \tag{59}$$

$$D_2^1 \alpha_2 = -\frac{\Gamma_{11}}{2\omega_b} + \frac{\Gamma_{22}}{2\omega_c} - \frac{\Gamma_{14} a_1^2}{8\omega_b} + \frac{\Gamma_{25} a_1^2}{8\omega_c} - \frac{\Gamma_{18} a_2^2}{8\omega_b}$$
$$+ \frac{\Gamma_{29} a_2^2}{8\omega_c} + \frac{b_{17} \cos \alpha_1}{2\omega_b a_1} + \frac{\Gamma_{21} a_1 \cos \alpha_2}{2\omega_c a_2} + \frac{\Gamma_{24} a_1^3 \cos \alpha_2}{8\omega_c a_2}$$
$$- \frac{\Gamma_{12} a_2 \cos \alpha_2}{2\omega_b a_1} - \frac{(\Gamma_{15} + \Gamma_{17}) a_1 a_2 \cos \alpha_2}{8\omega_b}$$
$$+ \frac{(\Gamma_{26} + \Gamma_{28}) a_1 a_2 \cos \alpha_2}{8\omega_c} - \frac{\Gamma_{19} a_2^3 \cos \alpha_2}{8\omega_b a_1} + \frac{\Gamma_{27} a_1^2 \cos 2\alpha_2}{8\omega_c}$$
$$- \frac{\Gamma_{16} a_2^2 \cos 2\alpha_2}{8\omega_b} - \frac{\Gamma_{13} a_3 \cos(\alpha_2 - \alpha_3)}{2\omega_b a_1}$$
$$+ \frac{\Gamma_{23} a_3 \cos \alpha_3}{2\omega_c a_2} + \frac{b_{23} \omega_b a_1 \sin \alpha_2}{2\omega_c a_2} + \frac{b_{213} \omega_d a_3 \sin \alpha_3}{2\omega_c a_2} \tag{60}$$

$$D_2^1 a_3 = -\frac{b_{31} a_3}{2} - \frac{b_{34} \omega_b a_1 \cos(\alpha_2 - \alpha_3)}{2\omega_d}$$
$$- \frac{b_{35} \omega_c a_2 \cos \alpha_3}{2\omega_d} + \frac{\Gamma_{31} a_1 \sin(\alpha_2 - \alpha_3)}{2\omega_d}$$
$$- \frac{\Gamma_{32} a_2 \sin \alpha_3}{2\omega_d} \tag{61}$$

$$D_2^1 \alpha_3 = \frac{\Gamma_{22}}{2\omega_c} - \frac{\Gamma_{33}}{2\omega_d} + \frac{\Gamma_{25} a_1^2}{8\omega_c} + \frac{\Gamma_{29} a_2^2}{8\omega_c} + \frac{\Gamma_{21} a_1 \cos \alpha_2}{2\omega_c a_2}$$
$$+ \frac{\Gamma_{24} a_1^3 \cos \alpha_2}{8\omega_c a_2} + \frac{\Gamma_{26} a_1 a_2 \cos \alpha_2}{8\omega_c}$$
$$+ \frac{\Gamma_{28} a_1 a_2 \cos \alpha_2}{8\omega_c} + \frac{\Gamma_{27} a_1^2 \cos 2\alpha_2}{8\omega_c} - \frac{\Gamma_{31} a_1 \cos(\alpha_2 - \alpha_3)}{2\omega_d a_3}$$
$$- \frac{\Gamma_{32} a_2 \cos \alpha_3}{2\omega_d a_3} + \frac{\Gamma_{23} a_3 \cos \alpha_3}{2\omega_c a_2}$$
$$+ \frac{b_{23} \omega_b a_1 \sin \alpha_2}{2\omega_c a_2} - \frac{b_{34} \omega_b a_1 \sin(\alpha_2 - \alpha_3)}{2\omega_d a_3} + \frac{b_{35} \omega_c a_2 \sin \alpha_3}{2\omega_d a_3}$$
$$+ \frac{b_{213} \omega_d a_3 \sin \alpha_3}{2\omega_c a_2} \tag{62}$$

where $\quad \alpha_1 = T_2 \sigma_1 - \Phi_1, \quad \alpha_2 = T_1 \sigma_2 + \Phi_1 - \Phi_2 \quad$ and $\alpha_3 = T_1 \sigma_3 - \Phi_2 + \Phi_3$. According to the method of reconstitution [10, 39], the equilibrium solutions are obtained by applying the vanishing of the variations of amplitude and phase on the actual non-dimensional timescale τ [10], i.e.

$$\begin{aligned} \dot{a}_m &= \varepsilon D_1^1 a_m + \varepsilon^2 D_2^1 a_m \\ \dot{\alpha}_m &= \varepsilon D_1^1 \alpha_m + \varepsilon^2 D_2^1 \alpha_m \end{aligned} \tag{63}$$

where ε is set equal to unity [40]. In particular, letting the coefficients b_{212} and b_{213} in Eqs. (51)–(62) equal to zero, the modulation equations of the beam and cable corresponding to Case 2 can be obtained and for the sake of simplicity, they are not presented in this paper. Substituting Eqs. (51)–(62) into Eq. (63) and letting $\dot{a}_m = \dot{\alpha}_m = 0$, the equilibrium solutions of the system can be sought by Newton–Raphson method and continued by pseudo-arclength algorithm [41]. The stability of the equilibrium solutions are evaluated by checking the eigenvalues of Jacobin matrix of the linearized system [42].

3 Numerical results and discussions

In this part, numerical results are discussed according to the theoretical solutions in the previous section. The corresponding parameters of the beam, cable and TMD are selected as follows. For the beam: the length is 300 m; mass per unit length is 48872 kg/m; cross-sectional area is 6.23m^2; the second moment of area is 3.2 m^4; Young's modulus is 200Gpa and the damping coefficient μ_b is 0.03. For the cable: the length is 200 m; mass per unit length is 48.62 kg/m; cross-sectional area is $3.0 \times 10^{-3} \text{ m}^2$; Young's modulus is 195Gpa; the initial force is 3.5×10^6 N; damping coefficient μ_c is 0.03; the angle between the cable and beam is 48°. The lower end of the cable is anchored at a distance of 24% from the right side of the beam (i.e., $s_1 = 0.76$). For the TMD: the stiffness of the spring is 9724 N/m; the mass is 486.2 kg (the mass ratio of TMD to cable is 5%); damping ratio ξ_d is 0.03. The TMD is installed at a distance of 4% from the lower end of the cable. In the following figures, SN and HB denote saddle-node and Hopf bifurcations,

respectively. In addition, stable solutions are depicted by solid lines, while unstable solutions are described by dashed lines.

3.1 Nonlinear behaviors of case 1: the cable-beam-TMD model

Figure 2 shows the frequency–response curves of the system when the excitation amplitude $F = 0.001$. The direct integration of Eqs. (20)–(22) is also performed by employing Runge–Kutta method. The corresponding results, represented by 'star' symbol, are utilized to verify the correctness of the perturbation solutions. There is a perfect agreement between the results of the two methods. It can be seen from Fig. 2 that the system exhibits a softening characteristic, because the response curves bend to the left. The bending of the curves results in the multivaluedness of the solutions. There are two peaks in each response curve, which makes the curve look like a 'saddle'. The left peak is commonly seen in a typical response curve of a cable, while the right one is related to internal resonance between the cable and TMD. Although the beam is not in direct contact with the TMD, the existence of the TMD still in turn has an obvious impact on the nonlinear behaviors of the beam through the internal resonance, since there is also a peak in the response curve of the beam. It can be concluded that the energy transfer between the beam, cable and TMD occurs near the right peak. When the excitation frequency (i.e., σ_1) is increased from a relatively small value, the response amplitudes increase correspondingly and lose their stabilities via the saddle-node (SN1), at which a jump up to the upper branch from the lower branch will take place. From this point on, the response amplitudes begin to decrease until they reach
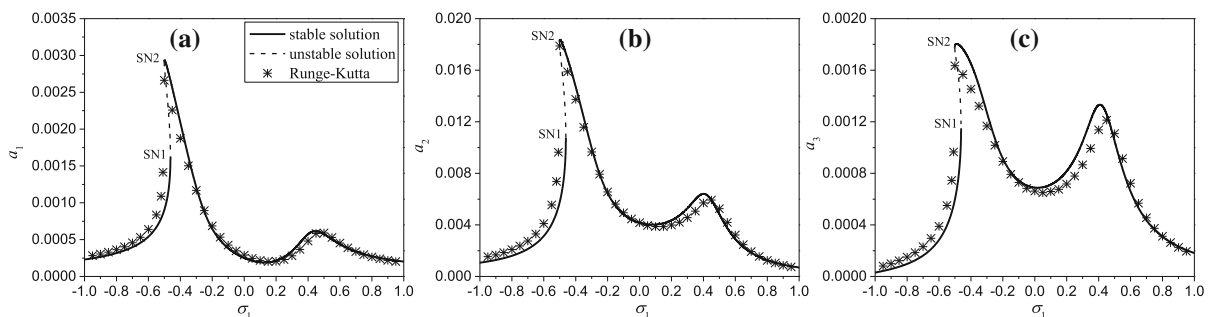
Fig. 2 The frequency–response curves of the system with $F = 0.001$, $\sigma_2 = 0.67$ and $\sigma_3 = -0.44$: **a** for beam, **b** for cable, **c** for TMD
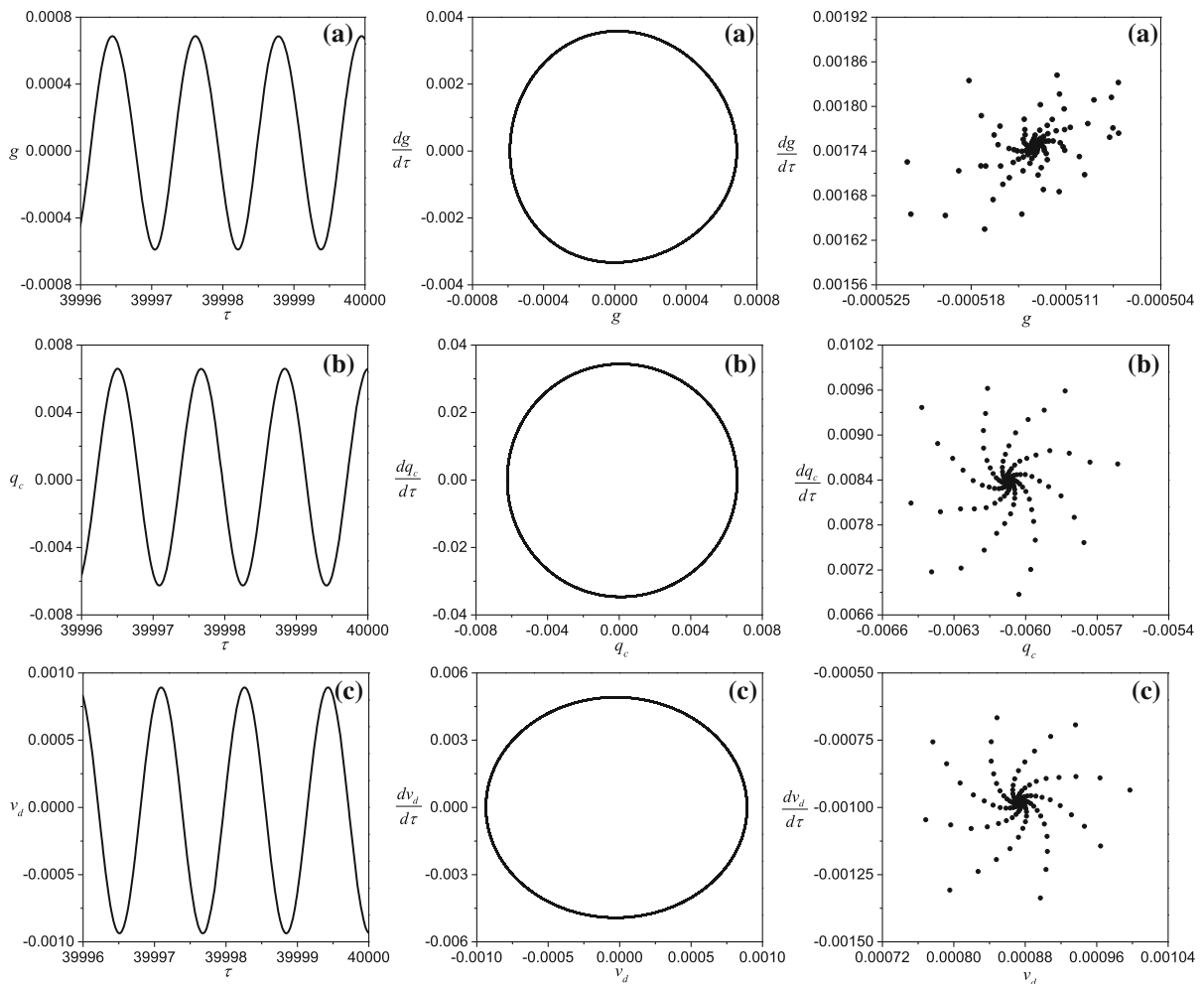
Fig. 3 Time-histories, phase portraits and Poincare sections of the system when $\sigma_1 = -0.2$ and $F = 0.001$: **a** for beam, **b** for cable, **c** for TMD

the bottom of the 'saddle'. With the further increase in σ_1, the amplitudes gradually increase up to the right peaks and then reduce. On the contrary, if the excitation frequency decreases from a relatively large value, the amplitudes increase to the right peaks first and then decrease to the bottom of the 'saddle'. As σ_1 is decreased further, the amplitudes increase accordingly until SN2 is reached. At this point, the jump phenomenon (from the upper branch to the lower branch) triggered by SN2 will happen. Thereafter, the amplitudes decrease slowly with decreasing σ_1.

Apart from the response curves, there are many other tools to study the nonlinear characteristics of the system, such as time-histories, phase portraits and Poincare sections, which can be obtained easily by

integrating Eqs. (20)–(22) directly via Mathematica software. Figure 3 illustrates the time-histories, phase portraits and Poincare sections of the system with excitation amplitudes $F = 0.001$. For the sake of simplicity, only $\sigma_1 = -0.2$ is given for an example. The initial values are chosen to be $g = 0.0001$, $\dot{g} = 0.01$, $q_c = 0.0001$, $\dot{q}_c = 0.01, v_d = 0.0001$, $\dot{v}_d = 0.01$. As can be seen in Fig. 3, the responses finally reach the steady state over an enough period of time. After reaching the steady state, the responses of the beam and cable are nearly synchronous (almost same phase), while those of the cable and TMD differ by a π phase. The phase portraits indicate that the periodic motions are described by one circle and there
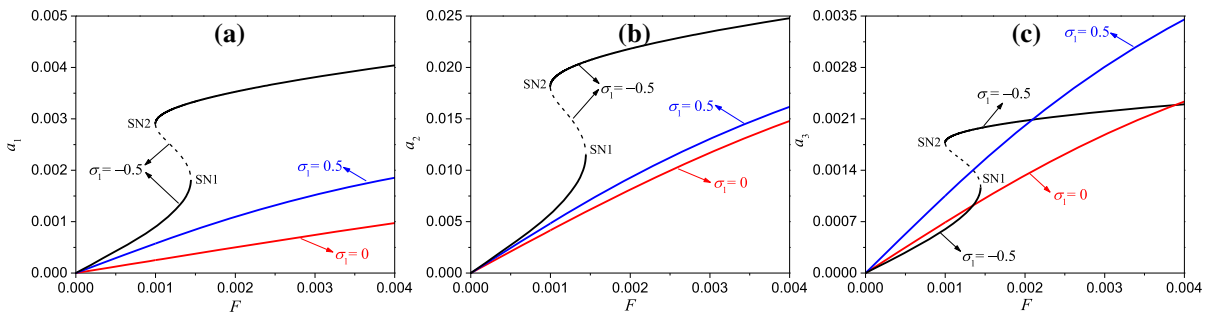
Fig. 4 Force-response curves of the system with different external detuning parameters when $\sigma_2 = 0.67$ and $\sigma_3 = -0.44$: **a** for beam, **b** for cable, **c** for TMD
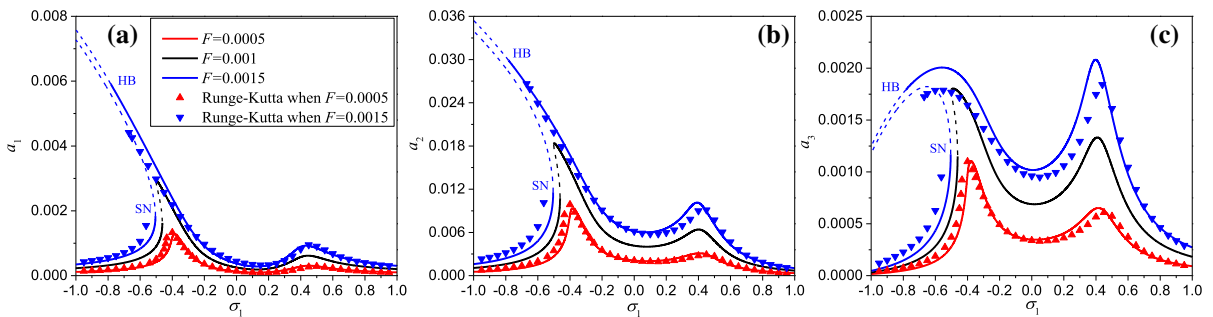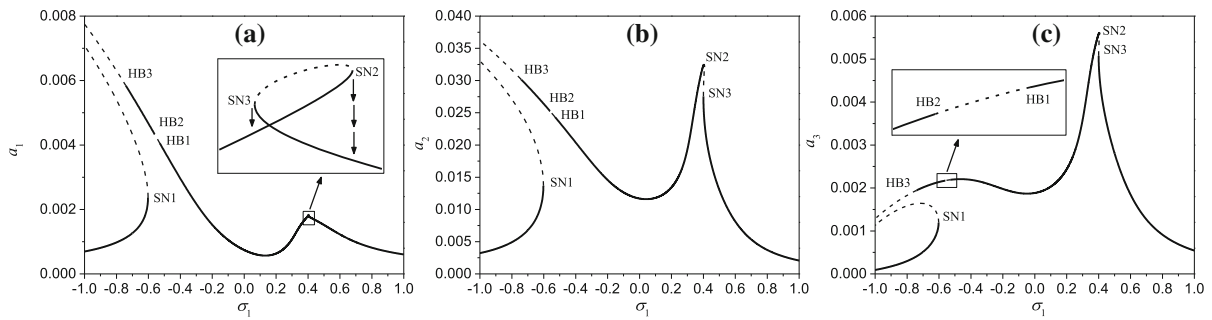

Fig. 5 The frequency–response curves of the system with different excitation amplitudes when $\sigma_2 = 0.67$ and $\sigma_3 = -0.44$: **a** for beam, **b** for cable, **c** for TMD

is only one clustered point in Poincare sections, which represents period-1 vibration.

Figure 4 shows the force-response curves of the system with external detuning parameter $\sigma_1 = -0.5, 0$ and 0.5, respectively. As can be seen in the figure, the multivalued phenomenon exists only when $\sigma_1 = -0.5$. In this circumstance, as excitation is increased from zero, the response amplitudes increase until they reach SN1. At this point, any slight increase in F will cause a jump from the lower branch to the upper branch. Afterwards, the response amplitudes increase with the further increase in excitation. Reversely, if the excitation is decreased from a relatively large value, the response amplitudes decrease correspondingly and the jump phenomenon triggered by SN2 will occur. When external detuning parameter is 0 and 0.5, the curves are relatively simple and a nearly linear relationship between the response and excitation can be observed. What's more, although the excitation is directly applied to the beam, the response of the cable is larger than those of the beam and TMD, because the parametric and forced vibration of the cable is

triggered by the motion of the beam as shown in Eq. (21).

Figure 5 gives the frequency–response curves of the system with different excitation amplitudes. The excitation amplitudes are chosen to be 0.0005, 0.001 and 0.0015, respectively. Meanwhile, the results obtained by Runge–Kutta method when $F = 0.0005$ and 0.0015 are also given. To make the graphs clear, the numerical results when $F = 0.001$ are not drawn in Fig. 5, since they have been presented in Fig. 2. The same reason, the saddle-nodes on the curves when $F = 0.001$ are not marked either. It can be seen that the agreement between the numerical results and perturbation solutions is satisfactory. Comparing the response curves under different excitation amplitudes, it is observed that the responses become larger when the system is subjected to a bigger excitation, because the system can attain more energy from external excitation. As the excitation amplitudes increase, the distance between the lower and upper branches expands, which indicates that the increase in excitation may lead to a larger resonance region. If the
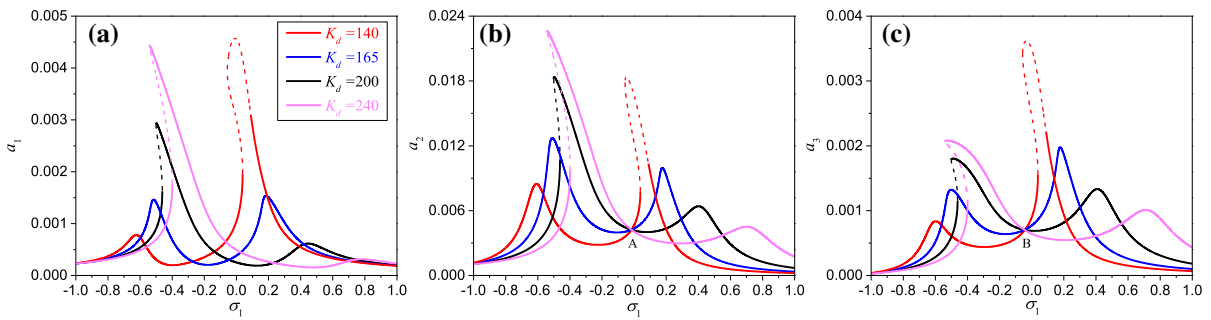
Fig. 6 The frequency–response curves of the system with $F = 0.003$, $\sigma_2 = 0.67$ and $\sigma_3 = -0.44$: **a** for beam, **b** for cable, **c** for TMD

excitation amplitude is relatively small (i.e., $F = 0.0005$), there are only stable solutions and the softening characteristic is weak. When $F = 0.001$, the softening characteristic is a little stronger compared to $F = 0.0005$. Additionally, there exist unstable solutions, which are connected to the stable solutions through two saddle-nodes (SN1 and SN2, see Fig. 2). If one goes on increasing the value of F (i.e., $F = 0.0015$), the softening characteristic becomes much stronger and the unstable regions expand. On the upper branch of the curve, the saddle-node vanishes, while a Hopf-bifurcation point (HB) appears, via which the stability of the solution changes. Observing Fig. 5c, it can be seen that if the excitation frequency is relatively small ($\sigma_1 < -0.55$), the response amplitude decreases with the decrease in σ_1 when $F = 0.0015$, which is different from those in Fig. 5a, b.

If the excitation amplitude is chosen to be a bit larger, namely, $F = 0.003$, an interesting phenomenon can be observed, as shown in Fig. 6. There are more bifurcation points on the response curves. In a small region near the right peak in Fig. 6a, two SNs (SN2 and SN3) appear. This actually leads to a double-jump phenomenon [30]. Imagine that the excitation frequency is increasing from a relatively small value and after the jump triggered by SN1, the response of the beam will vary along the curve in Fig. 6a until it reaches SN2, at which a jump from the upper to the lower will occur (as shown by the arrows in the enlarged part). On the other hand, if the excitation frequency is decreased from a value far above ω_b, a jump from the upper to the lower triggered by SN3 takes place (see the arrows in the enlarged part). The double-jump phenomena can also be observed in Fig. 6b, c. Nevertheless, the jump triggered by SN3 in

Fig. 6b, c is from the lower to the upper, which is different from Fig. 6a. Hence, the jump triggered by SN3 in Fig. 6a can be referred to as a reverse jump. Observing Fig. 6b (or Fig. 6c) can find that the left and right peaks exhibit different nonlinear characteristics because the left peak bend to the left and the right bend a little to the right. Recall that there are no bends of the right peaks in Fig. 5 and it can be concluded that a larger excitation may result in the nonlinearity of the right peak. Moreover, the value of right peaks of the cable and TMD in Fig. 6 increase sharply compared with Fig. 5. This indicates that more energy is transferred to the cable and TMD through internal resonance, which should attract our attention in practical engineering.

To explore the effect of the TMD on the nonlinear behaviors of the system, Fig. 7 gives the frequency–response curves of the system with different spring stiffness of the TMD. It should be noted that the bifurcation points are not marked in the figure, because they are not our focus. The phenomena as shown in Fig. 7 are very interesting. First, it can be seen that with the increase in stiffness, the values of the left peaks increase, while those of the right peaks decrease. The reason may be that as spring stiffness is increased, the absolute value of external detuning parameter (i.e., σ_1) corresponding to the left peaks becomes smaller, which implies a stronger relationship for the primary resonance. Meanwhile, the increase in spring stiffness leads to the increase in cable's frequency, which further results in a smaller difference between the frequencies of the beam and cable (i.e., a smaller internal detuning parameter σ_2). This means that the internal resonance relationship between the beam and cable will become stronger. In summary, stronger resonance relationships allow the

Fig. 7 The frequency–response curves of the system with different spring stiffness when $F = 0.001$: **a** for beam, **b** for cable, **c** for TMD
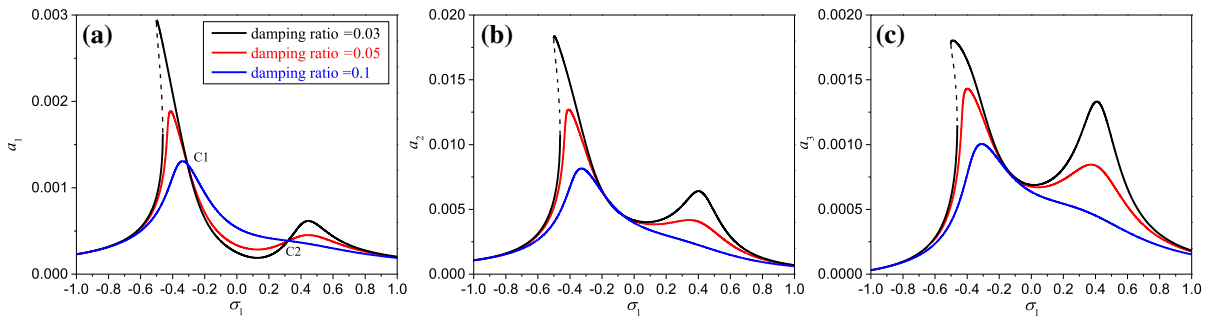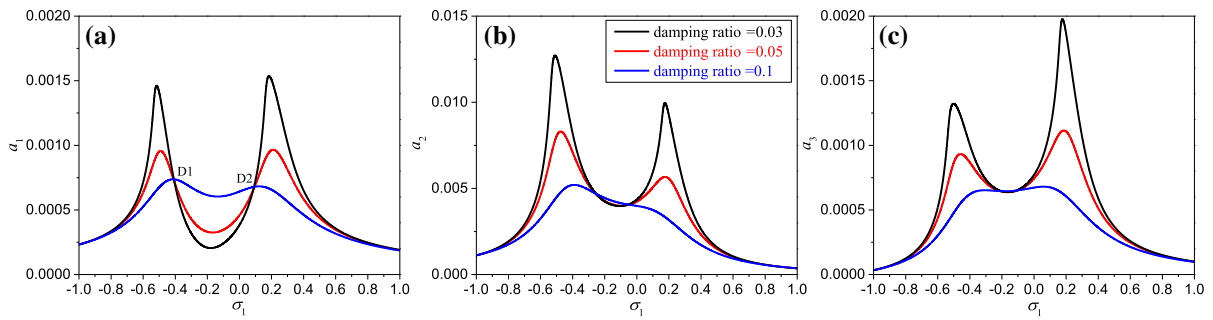

Fig. 8 The frequency–response curves of the system with different damping ratios of the TMD when $K_d = 200$ and $F = 0.001$: **a** for beam, **b** for cable, **c** for TMD

system to obtain more energy from external excitation. Hence, the values of the left peak increase with the increase in spring stiffness.

On the other hand, as spring stiffness is increased, the internal resonance relationship between the cable and TMD is stronger, because the absolute value of internal detuning parameter σ_3 is smaller. As mentioned before, the right peaks are related to the internal resonance between the cable and TMD, but why the right peaks become smaller rather than larger? It is because the external detuning parameters (i.e., σ_1) corresponding to the right peaks are bigger with the increase in spring stiffness. In this case, the primary resonance relationship is weaker and the energy transferred to the system from external excitation is limited. In other words, there is no enough energy input to maintain the large vibrations of the beam, cable and TMD at this time. Therefore, the right peaks decrease with the increase in spring stiffness although a stronger internal resonance relationship between the cable and TMD exists.

Another interesting phenomenon is that both of the left and right peaks move to the right with the increase

in spring stiffness and it seems that the whole curves shift to the right. Although the response amplitudes with different spring stiffness have various relationships when excitation frequency belongs to different range, there exists a minimum value between the left and right peaks. This may be used to control the associated vibration, but it is difficult to implement. After all, the cable-stayed bridge may be subjected to multi-frequency excitation in practical engineering. Observing Fig. 7b, c, two fixed points marked by 'A' and 'B' can be seen, which is first found by Den Hartog [43]. In other words, regardless of the change in spring stiffness, the response curve has to pass through the point 'A' (or 'B'). In addition, when spring stiffness is relatively small, i.e. $K_d = 140$, there are unstable solutions only on the right peaks. With the increase in stiffness, the response curves go through a variation process that unstable solutions on the right peaks vanish, while those on the left peaks appear. The process is continuous, since at a certain value of stiffness (i.e., $K_d = 165$), there is only stable solutions on the response curves, which is the transition of the process.

Fig. 9 The frequency–response curves of the system with different damping ratios of the TMD when $K_d = 165$ and $F = 0.001$: **a** for beam, **b** for cable, **c** for TMD
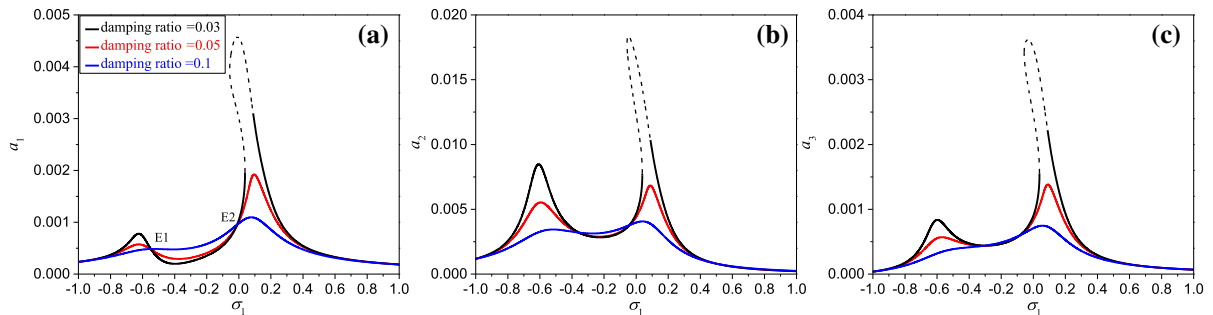
Fig. 10 The frequency–response curves of the system with different damping ratios of the TMD when $K_d = 140$ and $F = 0.001$: **a** for beam, **b** for cable, **c** for TMD

Figure 8 presents the frequency–response curves of the system with different damping ratios of the TMD. On the whole, the response amplitudes decrease with the increase in damping ratio, because a greater damping can consume more energy. Different from Fig. 7, both of the left and right peaks decrease, which indicates that the TMD has a good suppression on the vibration of the system. It is obvious that the damping of the TMD has a higher effect on the right peaks, since the right peaks nearly vanish when the damping ratio is increased to a relatively large value. From Fig. 8, it can be seen that as the damping ratio is increased, the unstable solutions disappear and the softening (hardening) characteristic becomes weaker. Moreover, two fixed points 'C1' and 'C2' are found in Fig. 8a, which is similar to the result in the reference [30].

Recall that the dynamic characteristics of the left and right peaks in Fig. 7 change with the variation of spring stiffness. Then what will happen if one changes the spring stiffness in Fig. 8? To explore this question, Figs. 9 and 10 give the frequency–response curves of the system with different damping ratios of the TMD

when $K_d = 165$ and 140, respectively. It can be seen from Fig. 9 that the damping has a great impact on both the left and right peaks and as the damping is increased, both peaks become much smaller. The responses of the points 'D1' and 'D2' are almost the same, which indicates that $K_d = 165$ may be near the optimal value for vibration suppression of the cable. Letting the responses of the two points 'D1' and 'D2' be equal, the parameters of the TMD can be further optimized [43]. In Fig. 10, the position of the lower fixed point 'E1' moves to the left and the damping has a larger impact on the left peaks, which is different from Fig. 8. Comparing Figs. 8, 9 and 10, it seems that the dynamic behaviors of the left and right peaks exchange when spring stiffness reaches a certain value.

In order to explore the nonlinear behaviors of the system near the fixed point, Fig. 11 is plotted. Figure 11 illustrates the time-histories and phase portraits of the beam near the point 'C2' in Fig. 8 when damping ratios of the TMD are different. The initial values are all $g = 0.0001$, $\dot{g} = 0.01$, $q_c = 0.0001$, $\dot{q}_c = 0.01$, $v_d = 0.0001$, $\dot{v}_d = 0.01$.
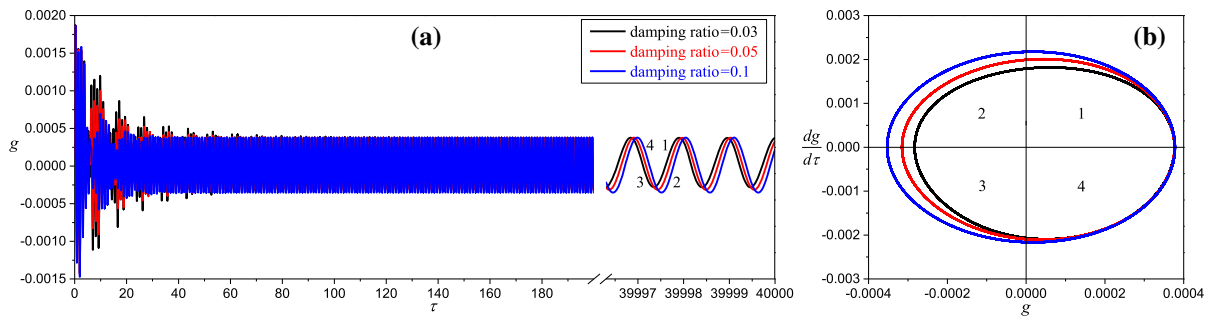
Fig. 11 The time-histories and phase portraits of the beam with different damping ratios of the TMD when $F = 0.001$: **a** time-histories, **b** phase portraits

Although the same initial values are chosen for the three damping ratios, however, the process through which the response reaches steady state is not identical. In addition, the 'beat vibration' [44] can be observed at the beginning of the oscillation because the frequencies of the cable and beam are close. After the steady state is reached, there exists a phase shift among the time-histories with different damping ratios, which may be the consequence of the TMD participating in coupling vibration. Furthermore, the steady-state responses are not symmetric about $g = 0$. In other words, the positive amplitudes are almost the same for different damping ratios. However, there exists a slight difference among the negative amplitudes. This can also be verified by phase portraits.

As shown in Fig. 11b, the phase portraits can be divided into four quadrants marked with '1, 2, 3 and 4', which corresponds to the segments '1, 2, 3 and 4' on the response curves, respectively. Only the arcs located in the fourth quadrant overlap each other. This indicates that when the responses are located in the fourth quadrant, the derivatives of the responses (i.e., the velocity or the tangent to the response corresponding to the segment '4') are also the same for different damping ratios, which is very interesting. The circles in Fig. 11b are not real ellipses, since they are not symmetric about the origin. The steady responses are not composed of a single harmonic wave, which is verified by the power spectrum. Figure 12 presents the power spectrum of the beam near the fixed point. For the sake of simplicity, only the case that damping ratio equal to 0.03 is given. As shown in the figure, two frequency components can be observed, one of which is extremely large (0.94 Hz), while the other one is very small (1.89 Hz). Noticing that the excitation
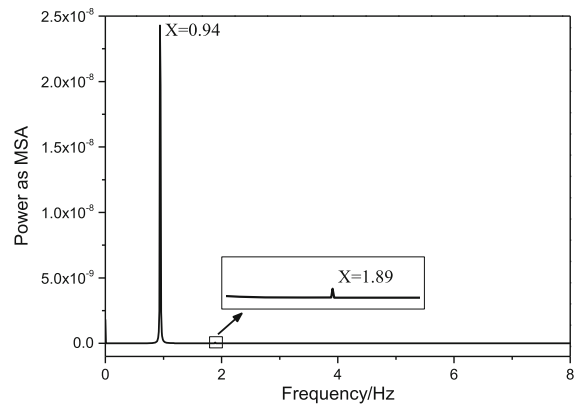

Fig. 12 Power spectrum of the beam near the fixed point with damping ratio = 0.03 and $F = 0.001$

frequency is 0.94 Hz, it can be learnt that in addition to the excitation frequency, twice the excitation frequency is also excited, which can be ignorable.

3.2 Compared with case 2: the cable-beam-TMD model without the vibration of the TMD

As known, the motion of the TMD actually adds one more DOF to the cable-beam-TMD model compared with the cable-beam system, which may cause the nonlinear behaviors of the model to differ significantly from those of the cable-beam system. Then how much does the motion of the TMD influence the nonlinear behaviors of the cable-beam system? To answer this question, this part discusses Case 2, namely, the cable-beam-TMD model without the vibration of the TMD ($v_d = 0$), which corresponds to considering only energy consumption. This can be achieved easily by letting the coefficients b_{212} and b_{213} in Eq. (21) equal to zero. Another reason for selecting Case 2 is based
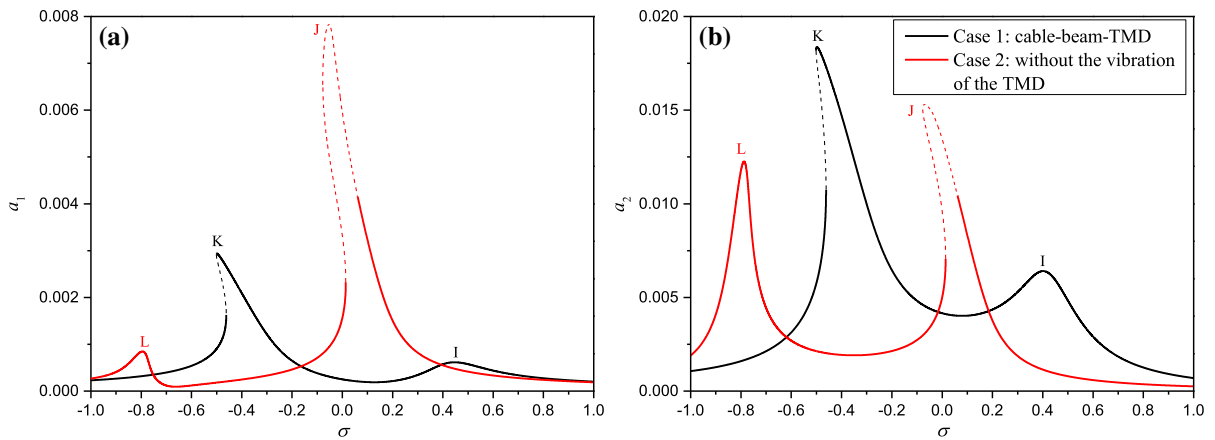
Fig. 13 Comparison between the frequency–response curves with/without the vibration of the TMD when $F = 0.001$: **a** for beam, **b** for cable
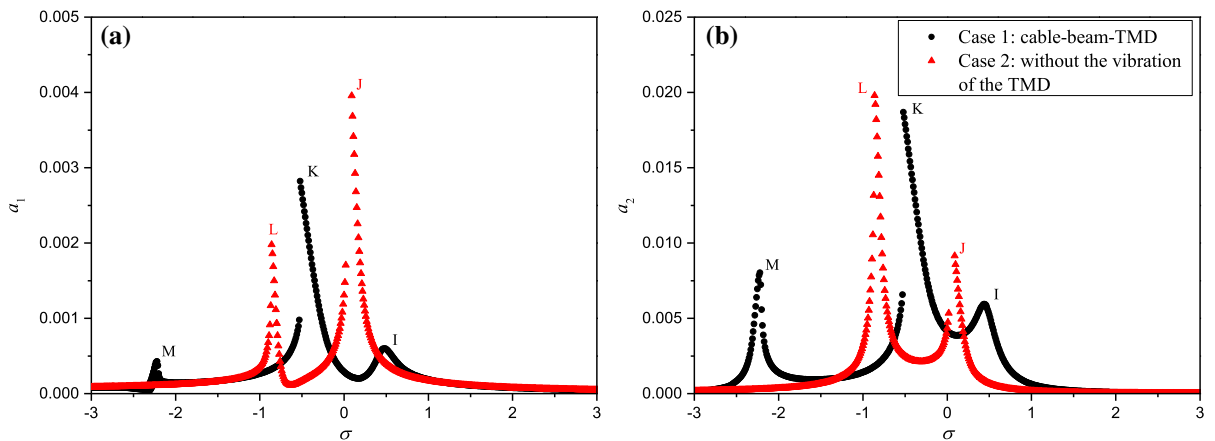

Fig. 14 Comparison between the frequency–response curves with/without the vibration of the TMD when $F = 0.001$ by directly integrating ODEs: **a** for beam, **b** for cable

on the following consideration. The spring stiffness will increase the fundamental frequency of the cable and to maintain the internal resonance conditions, the spring and damping of the TMD are retained.

Keeping our original intention in mind, Fig. 13 shows the comparison between the frequency–response curves with/without the vibration of the TMD. It can be seen that equipping the cable-beam system with a TMD cannot completely suppress the vibration of the beam and cable. The suppression effect of the TMD varies with different regions of excitation frequency, which may be caused by complex ways of energy transfer. Although there are two peaks on each curve of both cases, these peaks are fundamentally different. To explain this, let's turn our attention to Fig. 14, which gives the numerical solutions by

directly integrating the Eqs. (20)–(22) of both cases. It should be noted that the detuning range of excitation frequency in Fig. 14 is extended to [–3, 3]. As can be seen, there are actually three peaks in Case 1, but no matter how to increase the range of excitation frequencies, there are still only two peaks in Case 2. For the sake of description, the peaks are labelled with 'I, J, K, L and M', respectively.

First of all one can affirm that the peak 'I' of the beam (cable) disappears in Case 2, since the TMD don't vibrate and there is no internal resonance (energy transfer) between the cable and TMD in Case 2. Hence, the peaks 'K' and 'M' may correspond to the peaks 'J' and 'L', respectively. In other words, the TMD changes the positions of the peaks. This is not strange because the coefficients b_{212} and b_{213} have an
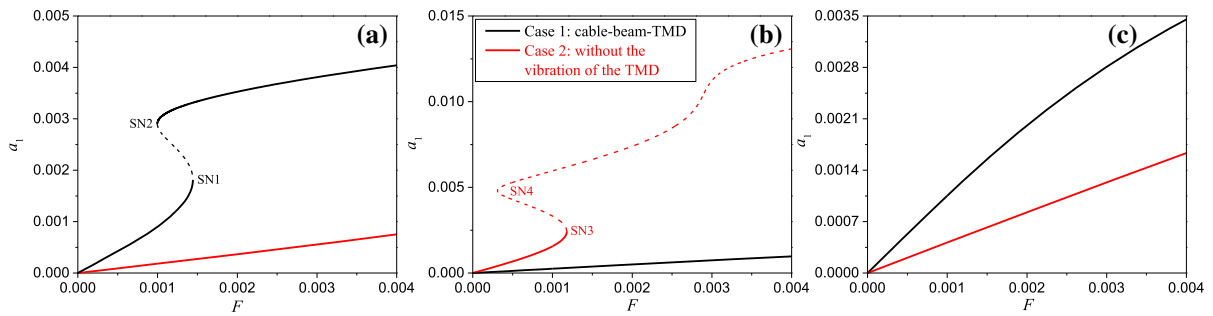
Fig. 15 Comparison between the force-response curves of the beam when there is (no) vibration of the TMD: **a** $\sigma_1 = -0.5$, **b** $\sigma_1 = 0$, **c** $\sigma_1 = 0.5$
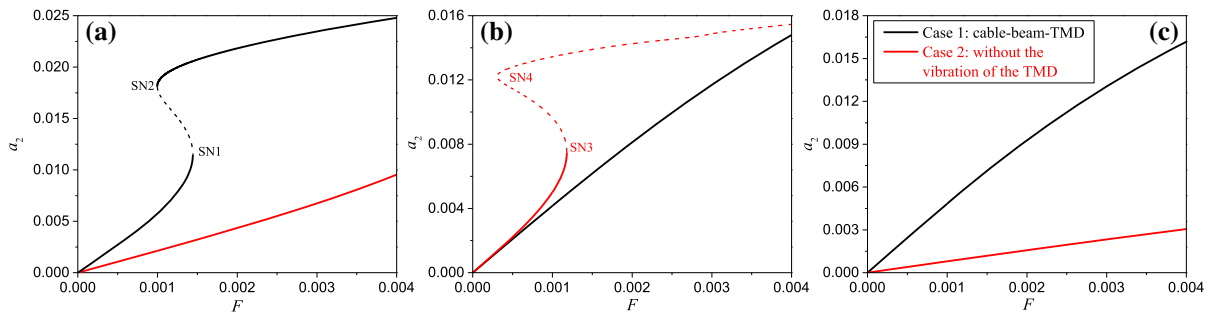

Fig. 16 Comparison between the force-response curves of the cable when there is (no) vibration of the TMD: **a** $\sigma_1 = -0.5$, **b** $\sigma_1 = 0$, **c** $\sigma_1 = 0.5$

obvious influence on the values of Γ_{13} and Γ_{21} to Γ_{23} as shown in Appendix B. Moreover, the value of the peak 'M' is smaller than that of the peak 'L', showing a good effect of vibration suppression. Compared with the peak 'J', the value of the peak 'K' is much smaller in Fig. 13a, while it is opposite in Fig. 13b. This means that more energy is transferred to the cable and TMD from the beam. Due to the offset of the positions of the peaks, one peak (peak 'M') disappears in our considered range of excitation frequency in Fig. 13. It can be learnt from the above phenomena that the TMD can reduce the peak values and even make some peaks disappear. But on the other hand, it is noted that the TMD may also lead to new peaks. In other words, TMD has both advantages and disadvantages from a nonlinear point of view. To further explore the difference between the two cases, Figs. 15 and 16 present the comparison between the force-response curves of the beam and cable. It can be seen that there are significant differences between the two curves in each graph except Figs. 15c and 16c. This means that in both cases, the response versus the excitation amplitude may exhibit completely different nonlinear

behaviors, which may be caused by the TMD being involved in the vibration. When the excitation frequency is distinct, the suppression effect of the two cases on the system is also different. For example, the suppression effect of Case 2 is better when $\sigma_1 = -0.5$ and 0.5. However, when $\sigma_1 = 0$, the suppression effect of Case 1 is better. The reason may be that the energy transfer among the beam, cable and TMD occurs. It can be learnt from above phenomena that the motion of the TMD has a great impact on the nonlinear behaviors of the system through internal resonance and energy transfer. Additionally, in Figs. 15b and 16b, a saddle-node bifurcation (SN4) that doesn't change the instability is observed. As mentioned in the reference [41], the half-branches meeting at SN4 are saddles and unstable nodes, both of which are all unstable. The similar phenomenon is also reported in the reference [30].

Figure 17 compares the time-histories and phase portraits when there is (no) vibration of the TMD. The initial values is the same with those in Fig. 3 and for the sake of simplicity, only the case that $\sigma_1 = -0.2$ is considered. It can be seen that there are obvious
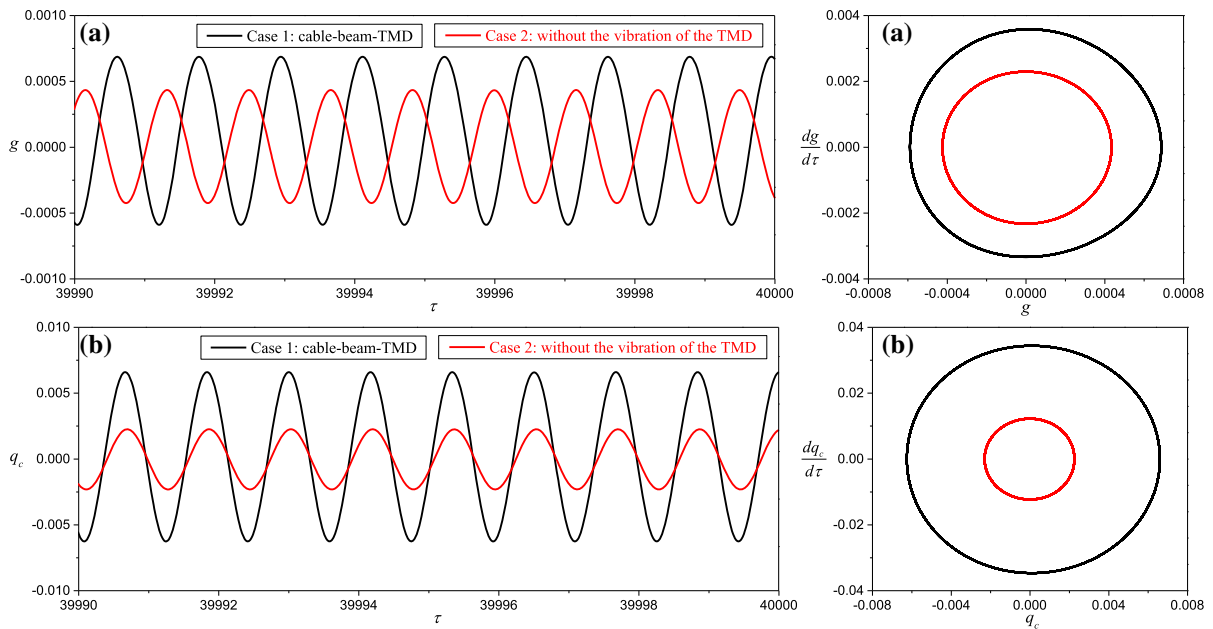
Fig. 17 Comparison of the time-histories and phase portraits of the system with $\sigma_1 = -0.2$ and $F = 0.001$ when there is (no) vibration of the TMD: **a** for beam, **b** for cable

differences between Fig. 17a, b. For example, the time-histories of the two cases in Fig. 17a are not synchronous. However, those in Fig. 17b are nearly synchronous, which may cause the phase portraits to look like a concentric ellipse. The above phenomena imply that the vibration of the TMD has different impacts on the nonlinear behaviors of the beam and cable.

4 Conclusions

Considering the vibration of the TMD, a cable-stayed beam with a TMD is studied. First, Galerkin's method is employed to discretize the differential equations of motion of the beam and cable, through which a set of ODEs are obtained. To solve the ODEs, the method of MTS is utilized and in this way, the modulation equations of the system are derived. Then, one of the stable solutions is sought by using Newton–Raphson method. Starting with the stable solution, the frequency/force-response curves are obtained by pseudo-arclength algorithm. The time-histories, phase portraits and Poincare sections are also presented to explore the effect of the TMD on the nonlinear behaviors of the system. Meanwhile, another case, i.e.,

the cable-beam-TMD model without the vibration of the TMD, is also investigated to reveal the role of the TMD in energy transfer. Finally, some interesting conclusions are drawn as follows.

1. Although there is no direct contact between the beam and TMD, there are still two peaks in the frequency–response curves of the beam. This indicates that the TMD has a significant influence on the nonlinear behaviors of the beam and energy transfer occurs among the beam, cable and TMD through internal resonance.

2. The increase in excitation amplitude will result in softening characteristic being stronger. With the increase in excitation amplitude, the saddle-node on the upper branch of the curve disappears, while a Hopf-bifurcation point arises. When excitation amplitude is relatively large, the right peaks exhibit nonlinearity and a reverse jump is observed. Meanwhile, the right peaks of the cable and TMD increase sharply.

3. With the increase in spring stiffness, both of the left and right peaks move to the right and their nonlinear characteristics are changed. The influence of the damping on the peaks is different for distinct spring stiffness. Despite the variation in spring stiffness and damping ratio of the TMD,

fixed points are found in the frequency–response curves.

4. TMD cannot completely suppress the vibration of the beam and cable from a nonlinear point of view. The suppression effect of the TMD varies with different regions of excitation frequency and the existence of the TMD changes the positions of the peaks. Although TMD can reduce the peak values and even eliminate some peaks, however, new peaks may also be introduced at the same time.

Data availability Data sharing not applicable to this article as no datasets were generated or analyzed during the current study.

Declarations

Conflict of interest The authors declare that they have no conflict of interests.

Appendix A

The expressions of the Galerkin integral coefficients in Eq. (20) are given as follows

$$b_{11} = \omega_b^2 = \frac{1}{\int_0^1 \phi_b^2(s)\mathrm{d}s}\left[\frac{\int_0^1 \phi_b(s)\phi_b''''(s)\mathrm{d}s}{\beta_b^4}\right.$$
$$+\gamma_c\psi_c\phi_b^2(s_1)\sin\theta\cos\theta\int_0^1 y_c'(x)\mathrm{d}x$$
$$\left.+\gamma_c\psi_c\phi_b^2(s_1)\sin^2\theta\right];$$

$$b_{12} = -\frac{\gamma_c^2\psi_c\phi_b^3(s_1)\cos^2\theta\sin\theta}{2\int_0^1 \phi_b^2(s)\mathrm{d}s};$$

$$b_{13} = -\frac{\eta_b}{\int_0^1 \phi_b^2(s)\mathrm{d}s}\frac{\int_0^1 \phi_b'(s)\phi_b'(s)\mathrm{d}s\int_0^1 \phi_b(s)\phi_b''(s)\mathrm{d}s}{2\beta_b^4};$$

$$b_{14} = -\frac{\psi_c\phi_b(s_1)\sin\theta\int_0^1 y_c'(x)\phi_c'(x)\mathrm{d}x}{\int_0^1 \phi_b^2(s)\mathrm{d}s};$$

$$b_{15} = \frac{\gamma_c\psi_c\phi_b^2(s_1)\sin\theta\cos\theta\int_0^1 \phi_c'(x)\mathrm{d}x}{\int_0^1 \phi_b^2(s)\mathrm{d}s};$$

$$b_{16} = -\frac{\psi_c\phi_b(s_1)\sin\theta\int_0^1 \phi_c'(x)\phi_c'(x)\mathrm{d}x}{2\int_0^1 \phi_b^2(s)\mathrm{d}s};$$

$$F = \int_0^1 F_1(s)\phi_b(s)\mathrm{d}s;$$

$$b_{17} = \frac{-F}{\int_0^1 \phi_b^2(s)\mathrm{d}s}.$$

The expressions of the Galerkin integral coefficients in Eq. (21) are given as follows

$$b_{21} = \omega_c^2 = \frac{1}{\int_0^1 \phi_c^2(x)\mathrm{d}x}\left[K_d\phi_c^2(l_1)\right.$$
$$-\frac{\lambda_c\int_0^1 y_c'(x)\phi_c'(x)\mathrm{d}x\int_0^1 y_c''(x)\phi_c(x)\mathrm{d}x}{\beta_c^2}$$
$$\left.-\int_0^1 \frac{\phi_c(x)\phi_c''(x)}{\beta_c^2}\mathrm{d}x\right];$$

$$b_{22} = \frac{1}{\int_0^1 \phi_c^2(x)\mathrm{d}x}\left[\mu_c\int_0^1 \phi_c^2(x)\mathrm{d}x + C_d\phi_c^2(l_1)\right];$$

$$b_{23} = \frac{1}{\int_0^1 \phi_c^2(x)\mathrm{d}x}\left[-\gamma_c\mu_c\phi_b(s_1)\cos\theta\right.$$
$$\left.\int_0^1 x\phi_c(x)\mathrm{d}x - C_d l_1\gamma_c\phi_b(s_1)\phi_c(l_1)\cos\theta\right]$$

$$b_{24} = -\frac{\gamma_c\phi_b(s_1)\cos\theta\int_0^1 x\phi_c(x)\mathrm{d}x}{\int_0^1 \phi_c^2(x)\mathrm{d}x};$$

$$b_{25} = \frac{1}{\int_0^1 \phi_c^2(x)\mathrm{d}x}\left[\frac{\lambda_c\gamma_c\phi_b(s_1)\cos\theta\int_0^1 y_c'(x)\mathrm{d}x\int_0^1 y_c''(x)\phi_c(x)\mathrm{d}x}{\beta_c^2}\right.$$
$$\left.+\frac{\lambda_c\gamma_c\phi_b(s_1)\sin\theta\int_0^1 y_c''(x)\phi_c(x)\mathrm{d}x}{\beta_c^2} - K_d l_1\gamma_c\phi_b(s_1)\phi_c(l_1)\cos\theta\right];$$

$$b_{26} = -\frac{1}{\int_0^1 \phi_c^2(x)\mathrm{d}x}\frac{\lambda_c\gamma_c^2\phi_b^2(s_1)\cos^2\theta\int_0^1 y_c''(x)\phi_c(x)\mathrm{d}x}{2\beta_c^2};$$

$$b_{27} = \frac{1}{\int_0^1 \phi_c^2(x)\mathrm{d}x}$$

$$\left[\frac{\lambda_c \gamma_c \phi_b(s_1) \cos\theta \int_0^1 \phi_c'(x)\mathrm{d}x \int_0^1 y_c''(x)\phi_c(x)\mathrm{d}x}{\beta_c^2} \right.$$

$$+ \frac{\lambda_c \gamma_c \phi_b(s_1) \cos\theta \int_0^1 y_c'(x)\mathrm{d}x \int_0^1 \phi_c(x)\phi_c''(x)\mathrm{d}x}{\beta_c^2}$$

$$\left. + \frac{\lambda_c \gamma_c \phi_b(s_1) \sin\theta \int_0^1 \phi_c(x)\phi_c''(x)\mathrm{d}x}{\beta_c^2} \right];$$

$$b_{28} = \frac{1}{\int_0^1 \phi_c^2(x)\mathrm{d}x}$$

$$\left[-\frac{\lambda_c \int_0^1 \phi_c'(x)\phi_c'(x)\mathrm{d}x \int_0^1 y_c''(x)\phi_c(x)\mathrm{d}x}{2\beta_c^2} \right.$$

$$\left. - \frac{\lambda_c \int_0^1 y_c'(x)\phi_c'(x)\mathrm{d}x \int_0^1 \phi_c''(x)\phi_c(x)\mathrm{d}x}{\beta_c^2} \right];$$

$$b_{29} = -\frac{1}{\int_0^1 \phi_c^2(x)\mathrm{d}x} \frac{\lambda_c \gamma_c^2 \phi_b^2(s_1) \cos^2\theta \int_0^1 \phi_c(x)\phi_c''(x)\mathrm{d}x}{2\beta_c^2};$$

$$b_{210} = \frac{1}{\int_0^1 \phi_c^2(x)\mathrm{d}x} \frac{\lambda_c \gamma_c \phi_b(s_1) \cos\theta \int_0^1 \phi_c'(x)\mathrm{d}x \int_0^1 \phi_c(x)\phi_c''(x)\mathrm{d}x}{\beta_c^2};$$

$$b_{211} = -\frac{1}{\int_0^1 \phi_c^2(x)\mathrm{d}x} \frac{\lambda_c \int_0^1 \phi_c'(x)\phi_c'(x)\mathrm{d}x \int_0^1 \phi_c(x)\phi_c''(x)\mathrm{d}x}{2\beta_c^2};$$

$$b_{212} = -\frac{K_d \phi_c(l_1)}{\int_0^1 \phi_c^2(x)\mathrm{d}x};$$

$$b_{213} = -\frac{C_d \phi_c(l_1)}{\int_0^1 \phi_c^2(x)\mathrm{d}x};$$

The expressions of the Galerkin integral coefficients in Eq. (22) are given as follows

$$b_{31} = 2\xi_d \omega_d;$$

$$b_{32} = l_1 \gamma_c \omega_d^2 \phi_b(s_1) \cos\theta;$$

$$b_{33} = -\omega_d^2 \phi_c(l_1);$$

$$b_{34} = 2l_1 \gamma_c \xi_d \omega_d \phi_b(s_1) \cos\theta;$$

$$b_{35} = -2\xi_d \omega_d \phi_c(l_1);$$

Appendix B

The expressions of the coefficients in Eq. (47) are defined as follows

$$\Gamma_{11} = \frac{b_{14}b_{25}}{4\omega_b \omega_c};$$

$$\Gamma_{12} = -\frac{b_{14}\sigma_2}{2\omega_b};$$

$$\Gamma_{13} = \frac{b_{14}b_{212}}{4\omega_b \omega_c};$$

$$\Gamma_{14} = -3b_{13} + \frac{10b_{12}^2}{3\omega_b^2} + \frac{2b_{15}b_{26}}{\omega_c^2} - \frac{b_{15}b_{26}}{4\omega_b^2 - \omega_c^2};$$

$$\Gamma_{15} = \frac{2b_{12}b_{15}}{\omega_b^2} - \frac{b_{15}b_{27}}{\omega_b(\omega_b - 2\omega_c)} + \frac{4b_{16}b_{26}}{\omega_c^2}$$
$$+ \frac{2b_{12}b_{15}}{(2\omega_b - \omega_c)\omega_c} - \frac{2b_{12}b_{15}}{\omega_c(2\omega_b + \omega_c)}$$
$$- \frac{b_{15}b_{27}}{\omega_b(\omega_b + 2\omega_c)};$$

$$\Gamma_{16} = -\frac{2b_{16}b_{27}}{\omega_b(\omega_b - 2\omega_c)} - \frac{b_{15}b_{28}}{3\omega_c^2} + \frac{b_{15}^2}{(2\omega_b - \omega_c)\omega_c}$$
$$- \frac{2b_{12}b_{16}}{-\omega_b^2 + 4\omega_c^2};$$

$$\Gamma_{17} = -\frac{b_{12}b_{15}}{3\omega_b^2} - \frac{b_{15}b_{27}}{\omega_b(\omega_b - 2\omega_c)} + \frac{2b_{12}b_{15}}{(2\omega_b - \omega_c)\omega_c}$$
$$- \frac{2b_{16}b_{26}}{4\omega_b^2 - \omega_c^2};$$

$$\Gamma_{18} = \frac{4b_{12}b_{16}}{\omega_b^2} - \frac{2b_{16}b_{27}}{\omega_b(\omega_b - 2\omega_c)} + \frac{2b_{15}b_{28}}{\omega_c^2}$$
$$+ \frac{b_{15}^2}{(2\omega_b - \omega_c)\omega_c} - \frac{b_{15}^2}{\omega_c(2\omega_b + \omega_c)}$$
$$- \frac{2b_{16}b_{27}}{\omega_b(\omega_b + 2\omega_c)};$$

$$\Gamma_{19} = \frac{2b_{15}b_{16}}{\omega_b^2} + \frac{10b_{16}b_{28}}{3\omega_c^2} - \frac{b_{15}b_{16}}{-\omega_b^2 + 4\omega_c^2};$$

The expressions of the coefficients in Eq. (48) are defined as follows

$$\Gamma_{21} = b_{24}\omega_b^2 + \frac{b_{25}\sigma_2}{2\omega_c} + \frac{b_{212}b_{32}}{4\omega_c \omega_d};$$

$$\Gamma_{22} = \frac{b_{14}b_{25}}{4\omega_b\omega_c} + \frac{b_{212}b_{33}}{4\omega_c\omega_d};$$

$$\Gamma_{23} = \frac{b_{212}\sigma_3}{2\omega_c};$$

$$\Gamma_{24} = \frac{10b_{12}b_{26}}{3\omega_b^2} + \frac{2b_{26}b_{27}}{\omega_c^2} - \frac{b_{26}b_{27}}{4\omega_b^2 - \omega_c^2};$$

$$\Gamma_{25} = -2b_{29} + \frac{2b_{12}b_{27}}{\omega_b^2} - \frac{b_{27}^2}{\omega_b(\omega_b - 2\omega_c)} + \frac{4b_{26}b_{28}}{\omega_c^2} + \frac{2b_{15}b_{26}}{(2\omega_b - \omega_c)\omega_c} - \frac{2b_{15}b_{26}}{\omega_c(2\omega_b + \omega_c)} - \frac{b_{27}^2}{\omega_b(\omega_b + 2\omega_c)};$$

$$\Gamma_{26} = -b_{210} - \frac{2b_{27}b_{28}}{\omega_b(\omega_b - 2\omega_c)} - \frac{b_{27}b_{28}}{3\omega_c^2} + \frac{b_{15}b_{27}}{(2\omega_b - \omega_c)\omega_c} - \frac{2b_{16}b_{26}}{-\omega_b^2 + 4\omega_c^2};$$

$$\Gamma_{27} = -b_{29} - \frac{b_{12}b_{27}}{3\omega_b^2} - \frac{b_{27}^2}{\omega_b(\omega_b - 2\omega_c)} + \frac{2b_{15}b_{26}}{(2\omega_b - \omega_c)\omega_c} - \frac{2b_{26}b_{28}}{4\omega_b^2 - \omega_c^2};$$

$$\Gamma_{28} = -2b_{210} + \frac{4b_{16}b_{26}}{\omega_b^2} - \frac{2b_{27}b_{28}}{\omega_b(\omega_b - 2\omega_c)} + \frac{2b_{27}b_{28}}{\omega_c^2} + \frac{b_{15}b_{27}}{(2\omega_b - \omega_c)\omega_c} - \frac{b_{15}b_{27}}{\omega_c(2\omega_b + \omega_c)} - \frac{2b_{27}b_{28}}{\omega_b(\omega_b + 2\omega_c)};$$

$$\Gamma_{29} = -3b_{211} + \frac{2b_{16}b_{27}}{\omega_b^2} + \frac{10b_{28}^2}{3\omega_c^2} - \frac{b_{16}b_{27}}{-\omega_b^2 + 4\omega_c^2};$$

The expressions of the coefficients in Eq. (49) are defined as follows

$$\Gamma_{31} = \frac{b_{32}\sigma_2}{2\omega_d} - \frac{b_{32}\sigma_3}{2\omega_d} + \frac{b_{25}b_{33}}{4\omega_c\omega_d};$$

$$\Gamma_{32} = -\frac{b_{33}\sigma_3}{2\omega_d} + \frac{b_{14}b_{32}}{4\omega_b\omega_d};$$

$$\Gamma_{33} = \frac{b_{212}b_{33}}{4\omega_c\omega_d}.$$

References

1. Ouni, M.H.E., Kahla, N.B., Preumont, A.: Numerical and experimental dynamic analysis and control of a cable stayed bridge under parametric excitation. Eng. Struct. **45**, 244–256 (2012)
2. Xu, L., Hui, Y., Yang, Q.S., Chen, Z.Q., Law, S.S.: Modeling and modal analysis of suspension bridge based on continual formula method. Mech. Syst. Sig. Process. **162**, 107855 (2022)
3. Su, X.Y., Kang, H.J., Guo, T.D.: A novel modeling method for in-plane eigenproblem estimation of the cable-stayed bridges. Appl. Math. Model. **87**, 245–268 (2020)
4. Guo, T.D., Kang, H.J., Wang, L.H., Liu, Q.J., Zhao, Y.Y.: Modal resonant dynamics of cables with a flexible support: a modulated diffraction problem. Mech. Syst. Sig. Process. **106**, 229–248 (2018)
5. Han, F., Deng, Z.C., Dan, D.H.: A novel method for dynamic analysis of complex multi-segment cable systems. Mech. Syst. Sig. Process. **142**, 106780 (2020)
6. Zhao, Y.B., Wang, Z.Q., Zhang, X.Y., Chen, L.C.: Effects of temperature variation on vibration of a cable-stayed beam. Int. J. Struct. Stab. Dyn. **17**, 1750123 (2017)
7. Irvine, H.M.: Cable Structures. Dover Publications, New York (1992)
8. Hagedorn, P., Schafer, B.: On non-linear free vibrations of an elastic cable. Int. J. Nonlinear Mech. **15**(4–5), 333–340 (1980)
9. Luongo, A., Rega, G., Vestroni, F.: Planar non-linear free vibrations of an elastic cable. Int. J. Nonlinear Mech. **19**(1), 39–52 (1984)
10. Rega, G., Benedettini, F.: Planar non-linear oscillations of elastic cables under subharmonic resonance conditions. J. Sound Vib. **132**(3), 367–381 (1989)
11. Lee, C., Perkins, N.C.: Three-dimensional oscillations of suspended cables involving simultaneous internal resonances. Nonlinear Dyn. **8**(1), 45–63 (1995)
12. Srinil, N., Rega, G., Chucheepsakul, S.: Large amplitude three-dimensional free vibrations of inclined sagged elastic cables. Nonlinear Dyn. **33**(2), 129–154 (2003)
13. Zhao, Y.Y., Wang, L.H., Chen, D.L., Jiang, L.Z.: Non-linear dynamic analysis of the two-dimensional simplified model of an elastic cable. J. Sound Vib. **255**(1), 43–59 (2002)
14. Lenci, S., Ruzziconi, L.: Nonlinear phenomena in the single-mode dynamics of a cable-supported beam. Int. J. Bifurcat. Chaos **19**(3), 923–945 (2009)
15. Peng, J., Xiang, M.J., Wang, L.H., Xie, X.Z., Sun, H.X., Yu, J.D.: Nonlinear primary resonance in vibration control of cable-stayed beam with time delay feedback. Mech. Syst. Sig. Process. **137**, 106488 (2020)
16. Fujino, Y., Warnitchai, P., Pacheco, B.: An experimental and analytical study of auto-parametric resonance in a 3DOF model of cable-stayed-beam. Nonlinear Dyn. **4**(2), 111–138 (1993)
17. Gattulli, V., Lepidi, M.: Localization and veering in the dynamics of cable-stayed bridges. Comput. Struct. **85**(21–22), 1661–1678 (2007)

18. Gattulli, V., Lepidi, M.: Nonlinear interactions in the planar dynamics of cable-stayed beam. Int. J. Solids Struct. **40**(18), 4729–4748 (2003)

19. Gattulli, V., Morandini, M., Paolone, A.: A parametric analytical model for non-linear dynamics in cable-stayed beam. Earthq. Eng. Struct. Dyn. **31**, 1281–1300 (2002)

20. Gao, D.L., Chen, W.L., Zhang, R.T., Huang, Y.W., Li, H.: Multi-modal vortex- and rain-wind-induced vibrations of an inclined flexible cable. Mech. Syst. Sig. Process. **118**, 245–258 (2019)

21. Krenk, S.: Vibrations of a taut cable with an external damper. J. Appl. Mech. **67**(4), 772–776 (2000)

22. Krenk, S., Nielsen, S.R.K.: Vibrations of a shallow cable with a viscous damper. Proc. R. Soc. Lond. A. **458**, 339–357 (2002)

23. Main, J.A., Jones, N.P.: Free vibrations of taut cable with attached damper. I: linear viscous damper. J. Eng. Mech. ASCE. **128**(10), 1062–1071 (2002)

24. Main, J.A., Jones, N.P.: Free vibrations of taut cable with attached damper. II: nonlinear damper. J. Eng. Mech. ASCE. **128**(10), 1072–1081 (2002)

25. Yu, Z., Xu, Y.L.: Non-linear vibration of cable–damper systems. Part I: formulation. J. Sound Vib. **225**(3), 447–463 (1999)

26. Xu, Y.L., Yu, Z.: Non-linear vibration of cable–damper systems. Part II: application and verification. J. Sound Vib. **225**(3), 465–481 (1999)

27. Wu, W.J., Cai, C.S.: Theoretical exploration of a taut cable and a TMD system. Eng. Struct. **29**(6), 962–972 (2007)

28. Cai, C.S., Wu, W.J., Shi, X.M.: Cable vibration reduction with a hung-on TMD system. Part I: theoretical study. J. Vib. Control. **12**(7), 801–814 (2006)

29. Wu, W.J., Cai, C.S.: Cable vibration reduction with a hung-on TMD system. Part II: parametric study. J. Vib. Control. **12**(8), 881–899 (2006)

30. Su, X.Y., Kang, H.J., Guo, T.D.: Modelling and energy transfer in the coupled nonlinear response of a 1:1 internally resonant cable system with a tuned mass damper. Mech. Syst. Sig. Process. **162**, 108058 (2022)

31. Luo, S., Yan, Q.S., Liu, H.J.: Design of mitigation damper with support flexibility for stay cable under bridge deck excitation. Appl. Mech. Mater. **238**, 714–718 (2012)

32. Liang, D., Sun, L.M., Cheng, W.: Effect of girder vibration on performance of cable damper for cable-stayed bridge. Eng. Mech. **25**(5), 110–116 (2008). (**In Chinese**)

33. Hui, Y., Law, S.S., Zhu, W.D., Wang, Q.: Internal resonance of structure with hysteretic base-isolation and its application for seismic mitigation. Eng. Struct. **229**, 111643 (2021)

34. Luongo, A., Zulli, D.: Mathematical Models of Beams and Cables. Wiley, New York (2013)

35. Casciati, F., Ubertini, F.: Nonlinear vibration of shallow cables with semiactive tuned mass damper. Nonlinear Dyn. **53**(1–2), 89–106 (2007)

36. Pacheco, B.M., Fujino, Y., Sulekh, A.: Estimation curve for modal damping in stay cables with viscous damper. J. Struct. Eng. **119**(6), 1961–1979 (1993)

37. Zhou, P., Li, H.: Modeling and control performance of a negative stiffness damper for suppressing stay cable vibrations. Struct. Control Health Monit. **23**(4), 764–782 (2016)

38. Johnson, E.A., Baker, G.A., Spencer, B.F., Fujino, Y.: Semiactive Damping of Stay Cables. J Eng Mech. ASCE. **133**(1), 1–11 (2007)

39. Wang, L.H., Peng, J., Zhang, X.Y., Qiao, W.Z., He, K.: Nonlinear resonant response of the cable-stayed beam with one-to-one internal resonance in veering and crossover regions. Nonlinear Dyn. **103**, 115–135 (2021)

40. Lacarbonara, W., Rega, G., Nayfeh, A.H.: Resonant nonlinear normal modes. Part I: analytical treatment for structural one-dimensional systems. Int. J. Nonlinear Mech. **38**(6), 851–872 (2003)

41. Seydel, R.: Practical Bifurcation and Stability Analysis. Springer, New York (2009)

42. Nayfeh, A.H., Balachandran, B.: Applied Nonlinear Dynamics. Wiley, New York (1995)

43. Den Hartog, J.P.: Mechanical Vibrations, 4th edn. McGraw-Hill, New York (1956)

44. Su, X.Y., Kang, H.J., Chen, J.F., Guo, T.D., Sun, C.S., Zhao, Y.Y.: Experimental study on in-plane nonlinear vibrations of the cable-stayed bridge. Nonlinear Dyn. **98**, 1247–1266 (2019)